Title: The secreted neuronal signal Spock1 regulates the blood-brain barrier

Authors: Natasha M. O'Brown[1*], Nikit B. Patel[1], Ursula Hartmann[2], Allon M. Klein[1], Chenghua Gu[3], Sean G. Megason[1*]

Affiliations:
[1] Department of Systems Biology, Harvard Medical School, 200 Longwood Ave, Boston, MA 02115, U.S.A.
[2] University of Cologne, Joseph-Stelzmann-Str. 52 50931 Cologne, Germany
[3] Howard Hughes Medical Institute, Department of Neurobiology, Harvard Medical School, 220 Longwood Ave, Boston, MA 02115, USA

* denotes corresponding author

Correspondence:

Natasha M. O'Brown (Natasha_obrown@hms.harvard.edu)
Department of Systems Biology, Harvard Medical School
Boston, MA 02115, U.S.A.

Sean G. Megason (megason@hms.harvard.edu)
Department of Systems Biology, Harvard Medical School
Boston, MA 02115, U.S.A.
(Phone) 617-432-7441

ABSTRACT

The blood-brain barrier (BBB) is a unique set of properties of the brain vasculature which severely restricts its permeability to proteins and small molecules. Classic chick-quail chimera studies showed that these properties are not intrinsic to the brain vasculature but rather are induced by surrounding neural tissue. Here we identify Spock1 as a candidate neuronal signal for regulating BBB permeability in zebrafish and mice. Mosaic genetic analysis shows that neuronally-expressed Spock1 is cell non-autonomously required for a functional BBB. Leakage in *spock1* mutants is associated with altered extracellular matrix (ECM), increased endothelial transcytosis, and altered pericyte-endothelial interactions. Furthermore, a single dose of recombinant SPOCK1 partially restores BBB function in *spock1* mutants by quenching gelatinase activity and restoring vascular expression of BBB genes including *mcamb*. These analyses support a model in which neuronally secreted Spock1 induces BBB properties by altering the ECM, thereby regulating pericyte-endothelial interactions and downstream vascular gene expression.

One-Sentence Summary: Spock1 is a signal secreted by neurons that induces barrier properties in the brain vasculature

INTRODUCTION

The blood-brain barrier (BBB) maintains a tightly controlled homeostatic environment in the brain that is required for proper neural function. BBB breakdown has been implicated in multiple neurodegenerative diseases including Alzheimer's, Parkinson's, and Huntington's Diseases (Sweeney et al., 2018). Conversely, the BBB also serves as an obstacle for effective drug delivery to the brain. Therefore there is great interest in generating a better understanding of how to therapeutically regulate its permeability, both to restore BBB function in neurodegeneration and to transiently open it for improved chemotherapeutic access for brain tumors. The BBB is a specialized property of the brain vasculature, which is composed of a thin, continuous layer of non-fenestrated endothelial cells with uniquely restrictive properties. Brain endothelial cells create the barrier via two primary cellular mechanisms: 1) specialized tight junction complexes that block the transit of small water-soluble molecules between cells and 2) reduced levels of vesicular trafficking or transcytosis to restrict transit through endothelial cells (Reese and Karnovsky, 1967). At a molecular level, functional barrier endothelial cells are differentiated from peripheral endothelial cells by high expression of the tight junction molecule Claudin-5 (Campbell et al.,

2008) and the fatty acid transporter Mfsd2a (Andreone et al., 2017; Ben-Zvi et al., 2014), and an absence of the fenestra and vesicle associated protein Plvap (Hallmann et al., 1995). Expression of substrate-specific influx and efflux transporters, which dynamically regulate the intake of necessary nutrients and the removal of metabolic waste products (Sanchez-Covarrubias et al., 2014; Umans et al., 2017), further enhances the selectivity of the BBB.

The restrictive properties of the BBB are not intrinsic to brain endothelial cells, but are induced and maintained by signals in the brain microenvironment during embryonic development (Stewart and Wiley, 1981). When avascularized quail neural tissue was transplanted into embryonic chicken gut cavities, the blood vessels ingressing from the non-barrier gut tissue obtained functional BBB properties, specifically both tight junctions and reduced levels of vesicles, resulting in Trypan blue tracer confinement within the blood vessels (Stewart and Wiley, 1981). Conversely, when avascularized quail somite tissue was transplanted into embryonic chick brain, the blood vessels ingressing from the neural tissue lost functional BBB properties, leaking tracer into the quail graft due to increased endothelial transcytosis and loss of tight junction function. These data show that signals from the neural microenvironment to the vasculature control barrier function. Furthermore, these microenvironmental signals are also required to actively maintain barrier properties throughout life (Guérit et al., 2021; Heithoff et al., 2021; Lyck et al., 2009; Urich et al., 2012).

Mural cells called pericytes share the endothelial basement membrane and comigrate with endothelial cells during neovascularization of the developing brain. This close interaction between pericytes and endothelial cells is required for both the initiation and continued maintenance of barrier properties (Armulik et al., 2010; Bell et al., 2010; Daneman et al., 2010). Astrocytes, glial cells found exclusively in the central nervous system, completely ensheath the vasculature with their endfeet in a polarized fashion (Abbott et al., 2006). Astrocytes arise late in embryonic development, after neurogenesis is complete, with the vast majority of gliogenesis occurring postnatally in rodents. Mammalian astrocytes are potent inducers of barrier properties in vitro and in vivo, and are required for BBB maintenance (Guérit et al., 2021; Heithoff et al., 2021; Janzer and Raff, 1987). While the necessity of these two cell types has been known for decades, canonical Wnt signaling arising from both neuronal and astrocytic sources is the only microenvironmental signal known to induce and maintain BBB function (Benz et al., 2019; Daneman et al., 2009; Guérit et al., 2021; Liebner et al., 2008; Martin et al., 2022; Stenman et al., 2008; Vanhollebeke et al., 2015; Wang et al., 2012, 2018). However in addition to its role in

95 regulating barrier properties, Wnt signaling also plays an important role in tip cell specification
96 and angiogenesis in the developing brain (Stenman et al., 2008; Vanhollebeke et al., 2015; Wang
97 et al., 2012). Furthermore, mouse endothelial cells are Wnt-responsive as early as E9.5 (Liebner
98 et al., 2008), preceding the acquisition of functional barrier properties (Daneman et al., 2009),
99 suggesting that other signaling may be acting in conjunction with or in addition to Wnt signaling
100 for the induction of BBB properties.
101
102 To further examine the molecular determinants of BBB development, we turned to the optically
103 transparent zebrafish system, which allows for imaging of the intact BBB in toto throughout
104 zebrafish development. Zebrafish brain endothelial cells express many of the same molecular
105 markers as mammalian brain endothelial cells, including Glut1, Cldn5, ZO-1, and Mfsd2a
106 (Guemez-Gamboa et al., 2015; Jeong et al., 2008; O'Brown et al., 2019; Umans et al., 2017;
107 Vanhollebeke et al., 2015; Xie et al., 2010). We previously characterized the molecular and
108 subcellular mechanisms of functional BBB development in zebrafish, and determined that the
109 zebrafish BBB becomes functionally mature by 5 days post fertilization (dpf) due to the
110 suppression of transcytosis rather than through the acquisition of tight junction function, which
111 was observed as early as 3 dpf (O'Brown et al., 2019). During these studies, we serendipitously
112 discovered a recessive viable mutant with profound forebrain and midbrain barrier leakage which
113 we identify here to be the neuronally produced and secreted proteoglycan Spock1. Using an array
114 of perturbations and imaging techniques, we uncover the range of Spock1 signaling to the
115 vasculature, and identify that mechanistically Spock1 signaling acts through control of the
116 pericyte-endothelial extracellular matrix (ECM) to control endothelial transcytosis.
117
118 **RESULTS**
119 **Identification and mapping of a spontaneous leaky mutant to *spock1***
120 We found a spontaneous recessive mutant that leaks both an injected 1 kDa Alexa Fluor (AF)
121 405 NHS Ester dye and a transgenic 80 kDa serum protein DBP-EGFP (Xie et al., 2010) into the
122 forebrain and midbrain as early as 3 days post fertilization (dpf) with no improvement in BBB
123 function throughout larval development (Figure 1A-E) or adulthood (Figure 1G). This increased
124 BBB permeability in homozygous mutants occurs in the absence of hemorrhage or vascular
125 patterning defects (Figure S1), or any reduction in viability or fertility. Time lapse imaging of
126 injected 10 kDa Dextran revealed a steady accumulation of Dextran in the brain parenchyma of
127 leaky mutants over the course of an hour (Figure S2), closely resembling the dynamics of Dextran

128 leakage observed in *mfsd2aa* mutants with increased endothelial transcytosis (O'Brown et al.,
129 2019).
130
131 To identify the mutation responsible for this leakage phenotype, we performed linkage mapping
132 on 5 dpf mutant and wild type siblings using bulk segregant RNAseq (Miller et al., 2013) and
133 identified a single peak at chr14:2205271-3513919 (GRCz11; Figures 1H and S3). Of the 14
134 genes within the linkage region (Figure S3), 8 were expressed at 5 dpf. Two of these genes were
135 differentially expressed, *csf1ra* and *gstp2* (Table S1), and one had several mutations that
136 segregated with the leakage phenotype, *spock1.* To test whether loss of any of these genes
137 conferred the increased BBB permeability, we assessed tracer leakage in mosaic crispants
138 (zebrafish larvae injected at the 1-cell stage with Cas9 protein and gene-specific sgRNAs) at 5
139 dpf and observed no BBB defects in 42 *gstp2* or 35 *csf1ra* crispants (data not shown). However,
140 when we assessed BBB function in *spock1* crispants, we observed a strong leaky phenotype in
141 26% of larvae (26/100 injected fish; Figure S3) and moderate leakage in 53% (53/100 injected
142 fish; Figure S3) as well as a few that displayed BBB leakage restricted to one midbrain
143 hemisphere (4/100 injected fish; Figure S3). Leakage in *spock1* crispants corresponded with a
144 loss of *spock1* expression (Figure S3). *Spock1* encodes a secreted protein of unclear function
145 named for its conserved protein domains: SPARC (Osteonectin), Cwcv And Kazal Like Domains
146 Proteoglycan 1 protein (also known as Testican-1). Spock1 has three predicted domains: 1) a
147 Kazal-type serine protease inhibitor, 2) an extracellular SPARC calcium-binding region, and 3) a
148 thyroglobulin type-1 repeat region, in addition to being decorated by both chondroitin sulfate (CS)
149 and heparan sulfate (HS) glycosaminoglycan (GAG) chains (Figure 1I) (Bonnet et al., 1996;
150 Edgell et al., 2004). Further sequencing of *spock1* confirmed a few point mutations in the SPARC
151 calcium-binding domain in the leaky fish (Figure 1I), including a T241A missense mutation and
152 two silent mutations at Q249 and G250, hereafter referred to as s*pock1*$^{hm41/hm41}$ mutants.
153
154 To validate that loss of Spock1 function causes the leakage phenotype in the spontaneous
155 mutants, we generated a stable null allele designated *spock1*^{hm43} using CRISPR mutagenesis
156 with two sgRNAs to completely delete the 5' UTR and start codon of *spock1* (Figure 1I). As
157 expected based on the 550 bp genomic deletion, *spock1*$^{hm43/hm43}$ fish do not express *spock1*
158 (Figure S4). Functional tracer leakage assays using 10 kDa Dextran revealed the same increased
159 BBB permeability specifically in the forebrain and the midbrain observed in the spontaneous
160 s*pock1*$^{hm41/hm41}$ mutants (Figure 1J-L). This increased BBB permeability was accompanied with
161 increased expression of the pathological marker of leaky endothelial cells *plvapb:EGFP* (Umans

et al., 2017) compared to the negligible levels observed in wild type siblings with a functional BBB (Figure 1M-O). Lastly, we crossed both lines to test for genetic complementation, and observed the leaky phenotype in *spock1*$^{hm41/hm43}$ compound heterozygotes (Figure 1P-S), further indicating that the initial spontaneous mutant acts via loss of Spock1 function.

Neuronal Spock1 signals to the vasculature within a short range

Given the necessity of Spock1 in determining BBB function, we next wanted to assess where *spock1* was expressed during BBB development. Using HCR fluorescent *in situ* hybridization, we determined that *spock1* mRNA is expressed throughout the developing central nervous system (CNS), including the entire brain, retina and spinal cord (Figures 2A and S4), and that this expression is unaltered in the spontaneous *spock1*$^{hm41/hm41}$ mutants (Figure S4). Closer examination of the fluorescent signal revealed co-localization with the neuronal marker *elavl3* and not the vascular marker *kdrl* (Figure 2D-G), similar to its predominantly neural expression in the developing mouse CNS (Charbonnier et al., 2000). Prior single-cell RNA sequencing (scRNA-seq) data (Raj et al., 2020) and our own also showed expression of *spock1* primarily in neurons and never in vascular endothelial cells (Figure S6). Taken together, these data indicate that we have identified a neuronal signal, Spock1, that plays a role in establishing endothelial BBB properties during development without altering vascular patterning.

To determine the range of the Spock1 signal, we performed cell transplantation experiments to make genetically mosaic zebrafish embryos and assessed tracer leakage in relationship to the closest transplanted cells at 5 dpf (Figure 2H). When we transplanted labeled wild type cells into wild type host embryos, we observed a negligible level of tracer accumulation in the brain parenchyma regardless of the proximity of the nearest donor cell (Figure 2I and 2L). In contrast, when we transplanted *spock1*$^{hm41/hm41}$ mutant cells into mutant host embryos, we observed high levels of tracer accumulation in the parenchyma regardless of the proximity of the nearest donor cell (Figure 2J and 2L). Strikingly, when we transplanted wild type cells into *spock1* mutant hosts, we observed a complete rescue of the mutant leakage if the wild type donor cell was within 10 µm of a blood vessel and no rescue if the donor cell was more than 20 µm away (Figure 2K-N), indicating that Spock1 can functionally signal at a distance of 10 to 20 µm. Importantly, wild type cells could rescue leakage in mutant hosts when they differentiate as neurons but not endothelial cells (Figure 2M).

195 **Mutant leakage arises from increased transcytosis and altered pericyte-endothelial**
196 **interactions**
197 To assess the subcellular mechanism of increased BBB permeability in *spock1*$^{hm41/hm41}$ mutants,
198 we injected electron-dense NHS-gold nanoparticles (5 nm) into circulation, followed by
199 transmission electron microscopy (TEM) imaging in 7 dpf *spock1* mutant and wildtype siblings.
200 These TEM leakage assays revealed no alterations in the cellular composition of the
201 neurovascular unit (NVU) in *spock1* mutants, with endothelial cells and pericytes sharing a
202 basement membrane that is surrounded by neurons and glia (Figure 3A and 3B). A modest
203 impairment in tight junction function was observed in *spock1* mutants (52/59 functional tight
204 junctions; Figure 3D) compared to wild type siblings (57/57; Figure 3C). However, *spock1*
205 mutants had a significant increase in both small (<100 nm diameter) non-clathrin coated vesicles
206 (Figure 3D and 3G) and large (>200 nm diameter) vesicles (Figure 3F and 3H) suggesting that
207 the leakage results primarily from an increase in vesicular trafficking across endothelial cells. In
208 addition to the increase in total large vesicular abundance in *spock1* mutants, we also observed
209 several of these large vesicles fused to the abluminal membrane in multiple larvae with a few
210 examples of the gold nanoparticles visibly spilling into the endothelial basement membrane
211 (Figure 3F). Although pericyte coverage of the endothelium was unaltered (Figure S1), *spock1*
212 mutants displayed overall thinner pericyte-endothelial basement membranes with several
213 pericytes having long stretches of apparently direct contact on endothelial cells (Figure 3I-K),
214 corresponding with observations by live confocal microscopy (Figure S1). These data suggest
215 that loss of Spock1 function alters the critical pericyte extracellular interactions with endothelial
216 cells, resulting in loss of BBB properties as observed in pericyte-deficient mice and zebrafish
217 (Armulik et al., 2011; Bell et al., 2010; Daneman et al., 2010; Wang et al., 2013).
218
219 One of the proposed roles of Spock1 is to regulate matrix metalloproteinase (MMP) activation,
220 specifically gelatinases MMP-2 and MMP-9 (Du et al., 2020; Edgell et al., 2004; Nakada et al.,
221 2001; Váncza et al., 2022; Ye et al., 2020). To assess whether *spock1*$^{hm41/hm41}$ mutants had altered
222 gelatinase activity that corresponded to observed changes in vascular cell interactions, we
223 performed *in vivo* gelatin zymography by intracranial injections of highly quenched FITC-gelatin.
224 Proteolytic cleavage of FITC-gelatin by either MMP-2 or 9 releases bright FITC peptides resulting
225 in a non-reversible increase in fluorescence. This increase in fluorescence upon digestion is
226 proportional to the proteolytic activity of the MMPs, allowing for the detection of gelatinase activity
227 *in vivo* (Garcia-Alloza et al., 2009; Underly et al., 2017). Using this assay, we were able to see
228 that in wild type 5 dpf fish, the majority of the signal appears strongly in the cerebral spinal fluid

229 (CSF) and more subtly in many pericytes (Figure 3L). While *spock1*$^{hm41/hm41}$ mutants also
230 displayed strong gelatinase activity in the CSF, this was accompanied by a regional increase in
231 gelatinase activity specifically in the forebrain and midbrain (Figure 3M and 3N), the same regions
232 that were also prone to tracer accumulation (Figure 1). These data suggest that Spock1 helps
233 induce barrier function by keeping gelatinase activity in check.
234
235 **Spock1 plays a conserved role in inducing barrier function in mammals**
236 To determine if Spock1 plays a conserved role in determining vertebrate BBB properties, we
237 assessed BBB function in embryonic day 15.5 (E15.5) *Spock1*$^{-/-}$ mice (Röll et al., 2006) (Figure
238 4A), a stage when the cortex BBB is fully functional (Ben-Zvi et al., 2014). While wild type siblings
239 confined both 550 Da Sulfo-NHS-Biotin (Figure 4B) and 10 kDa Dextran (Figure 4D) within the
240 brain vasculature, *Spock1*$^{-/-}$ mice leaked both tracers into the cortex parenchyma (Figure 4C-G).
241 This increased BBB permeability was also associated with increased expression of the PLVAP
242 (Figure 4H-L), as seen in the zebrafish mutants (Figure 1N). These data indicate the Spock1 plays
243 a conserved role in inducing barrier properties during embryonic development. However, when
244 we repeated these leakage assays in adult mice, we observed full recovery in BBB function in
245 *Spock1*$^{-/-}$ mice (Figure S5). This contrasts with adult zebrafish *spock1*$^{hm41/hm41}$ mutants, which have
246 a defective BBB (Figure 1), indicating species-specific differences in the adult BBB.
247
248 **Vascular cells are the only altered cell types in *spock1* mutant brains**
249 To determine how Spock1, a neuronally produced and secreted proteoglycan, signals to and
250 regulates brain endothelial cell BBB properties, we turned to scRNA-seq of dissected 5 dpf
251 *spock1*$^{hm41/hm41}$ mutant and wild type brains, allowing us to globally assess cell type specific
252 molecular changes occurring in the mutant brains. With Leiden clustering of the scRNA-seq data
253 we defined cell clusters containing neurons, glial, and vascular cell types (Figure S6). We
254 performed differential gene expression (DGE) analysis for each cluster and did not observe any
255 changes in the neuronal or glial populations, but did observe significant changes in the vascular
256 cluster (Table S2). When we subclustered the vascular population, we were able to resolve
257 endothelial cells, pericytes and vascular smooth muscle cells (vSMCs; Figure 5A). Due to the
258 low vascular cell numbers present in the scRNA-seq data, we prioritized candidate genes for
259 subsequent validation by their fold-change in gene expression rather than statistical significance.
260 These analyses suggested molecular changes in the mutant endothelial cells indicative of a leaky
261 phenotype, with increased expression of *plvapb* and decreased expression of the tight junction
262 protein *cldn5b* (Figure 5B, Table S3). Interestingly, *spock1* mutants had decreased expression of

263 the melanoma cell adhesion molecule *mcamb* (also known as CD146) in both endothelial cells
264 and pericytes (Figure 5B and 5C). This decreased expression in the vasculature was validated
265 by HCR FISH, with minimal expression in mutant midbrain pericytes but normal levels in hindbrain
266 pericytes, which maintain BBB function in *spock1*$^{hm41/hm41}$ mutants (Figure 5D-G). CD146 has
267 previously been shown to be required for BBB integrity, as *CD146*$^{-/-}$ mice exhibit BBB breakdown
268 due to decreased pericyte coverage and downstream loss of endothelial expression of Cldn5
269 (Chen et al., 2017).
270
271 **Exogenous SPOCK1 restores barrier function**
272 To test the ability of Spock1 to rescue the mutant leakage phenotype, we injected recombinant
273 human SPOCK1 (rSPOCK1) protein directly into the brain of *spock1*$^{hm41/hm41}$ mutant larvae at 5
274 dpf and assessed brain permeability at 6 dpf. While control animals injected with PBS maintained
275 high levels of brain permeability (Figure 6A), larvae that received at least 2.3 ng of rSPOCK1 per
276 mg fish body weight showed a 50% reduction in brain permeability following a single dose (Figure
277 6B and 6C). These results further confirm that SPOCK1 is able to act cell non-autonomously to
278 rescue the mutant BBB leakage, as these injections were targeted broadly to the neural tissue
279 rather than the endothelial cells, and demonstrate functional conservation of Spock1 from human
280 to zebrafish.
281
282 To determine whether this restoration of barrier function corresponds to Spock1's regulation of
283 the MMP activity, we repeated the intracranial injections of 11.5 ng rSPOCK1/mg of fish in
284 *spock1*$^{hm41/hm41}$ mutants at 4 dpf and assessed barrier function and gelatinase activity at 5 dpf.
285 While 5 dpf control injected *spock1*$^{hm41/hm41}$ mutants continued to display high levels of BBB
286 permeability and gelatinase activity, rSPOCK1 reduced mutant leakage of 10 kDa Dextran about
287 50% (Figure 6E and 6F), just as it did when we injected rSPOCK1 at 5 dpf and assessed BBB
288 function at 6 dpf (Figure 6C). This restoration of BBB function was accompanied by a decrease
289 in gelatinase activity (Figure 6H and 6I). Finally, to determine whether Spock1 lies upstream of
290 vascular expression of the cell adhesion molecule *mcamb,* we assessed *mcamb* expression in
291 the mutant midbrain vasculature at 5 dpf with or without the addition of rSPOCK1. While
292 *spock1*$^{hm41/hm41}$ mutants injected with PBS displayed negligible levels of *mcamb* expression in the
293 midbrain (Figure 6J), mutants injected with rSPOCK1 had a 50% increase in *mcamb* expression
294 in the vasculature (Figure 6K and 6L), with a noticeable increase in *mcamb*+ pericytes.
295 Interestingly this 50% increase in *mcamb* expression directly correlates with the 50% reduction in
296 leakage and gelatinase activity following rSPOCK1 injections (Figure 6F and 6I).

297
298
299 **Discussion**
300
301 Together these data show that Spock1 is a secreted, neuronally expressed extracellular signal
302 that regulates BBB permeability in zebrafish and mouse without altering vascular patterning
303 during development (Figures 1 and 4). Mechanistically, this work suggests a model whereby
304 Spock1 regulates the brain extracellular environment via its inhibition of gelatinase activity,
305 thereby providing the appropriate chemical or mechanical signals for vascular pericytes and
306 endothelial cells to communicate properly with one another. This critical pericyte-endothelial
307 interaction thereby prompts a BBB transcriptional program, including increased expression of tight
308 junction (*cldn5b)* and cell adhesion (*mcamb*) molecules, decreased expression of leaky
309 endothelial genes (*plvapb*), and reduced transcytosis. Thus, loss of Spock1 function contributes
310 to increased BBB permeability by disruption of the complex extracellular scaffold that surrounds
311 and supports the vasculature during development. Together this work reveals how a novel signal
312 from the brain microenvironment can regulate the vasculature to give rise to the special properties
313 of the BBB and provides new targets for its therapeutic modulation.
314
315 Despite the ubiquitous expression of *spock1* throughout the CNS, *spock1* loss of function
316 zebrafish mutants display regional leakage in the forebrain and midbrain and a completely intact
317 hindbrain barrier. Spock1 is not alone in having region-specific regulation of barrier properties
318 despite pan-CNS expression. A recent study demonstrated that the pericyte-produced ECM
319 molecule vitronectin is required for functional retinal and cerebellar barriers despite its expression
320 by all CNS pericytes (Ayloo et al., 2022). Even mutants in canonical Wnt signaling have varying
321 levels or regionalized angiogenic or barrier defects despite wide-spread sources of Wnt signals
322 and receptors throughout the brain (Cho et al., 2017; Junge et al., 2009; Wang et al., 2012, 2018;
323 Xu et al., 2004; Zhou and Nathans, 2014; Zhou et al., 2014). Interestingly, the regions with the
324 highest susceptibility to single gene mutations in canonical Wnt signaling are the retina and the
325 cerebellum, while the cortex can maintain a functional BBB even with mutations in several genes
326 in the Wnt pathway (Wang et al., 2018). These data suggest that different regions of the brain are
327 either molecularly or cellularly (or both) distinct, perhaps in nuanced ways that are often masked
328 by current detection methods. For example, while the neurovascular unit of endothelial cells and
329 pericytes in close contact with astrocytic endfeet appears uniform throughout the brain by
330 immunostaining and EM, various scRNA-seq datasets have now shown that astrocytes are highly

331 regionally distinct at a molecular level (Herrero-Navarro et al., 2021; Ohlig et al., 2021; Zhu et al.,
332 2018) raising the possibility that they may respond to different signals. Pericytes in the brain,
333 unlike in the rest of the body, arise from two discrete origins, mesodermal and neural crest (Ando
334 et al., 2016; Trost et al., 2016). In zebrafish, the two origins have discrete domains, with the
335 hindbrain being exclusively derived from mesodermal origins and the midbrain and forebrain
336 being predominantly of neural crest origin (Ando et al., 2016) which interestingly matches the
337 leakage boundaries in *spock1* mutants.
338
339 Here we demonstrate that Spock1 regulates brain endothelial cell identity to initiate the barrier
340 program during development, both at molecular and subcellular resolution. However, this does
341 not preclude the fact that other brain barriers may be similarly affected by loss of this signal. In
342 addition to the BBB, the neural tissue is also protected by the blood-cerebrospinal fluid (CSF)
343 barrier, which is created by the choroid plexus epithelial cells lining the brain ventricles (Wolburg
344 and Paulus, 2010), and the arachnoid barrier, which is created by the epithelial cells beneath the
345 dura that completely enwrap the brain (Abbott, 2004). These various brain barriers mature on
346 different developmental timelines, with the blood-CSF barrier becoming impermeable by 4 dpf
347 (Henson et al., 2014), then the BBB by 5 dpf (O'Brown et al., 2019), and the arachnoid barrier
348 maturing after 9 dpf (Jeong et al., 2008) in zebrafish. While the focus of our study has been the
349 BBB, it is possible that these additional brain barriers also play a role in the observed leakage of
350 various tracers into the brain in *spock1* mutants.
351
352 The N-terminal region of Spock1 has previously been shown to regulate matrix metalloproteinase
353 (MMP) activity, specifically gelatinases MMP-2 and 9 (Du et al., 2020). We show here that leaky
354 *spock1*$^{hm41/hm41}$ mutants have increased gelatinase activity in the midbrain occurring in the same
355 place as the observed decrease in the endothelial-pericyte basement membrane (Figure 3 and
356 S1), suggesting that this excessive MMP activity may be responsible for the breakdown of the
357 basement membrane. Although all the cells in the neurovascular unit secrete MMP-2 and 9,
358 pericytes have recently been shown to produce MMP-9 in response to ischemia and TGF-β1
359 exposure, leading to increased barrier breakdown and neuronal damage (Takahashi et al., 2014;
360 Underly et al., 2017). For this reason, many have proposed gelatinases as a therapeutic target
361 for several neurological diseases that are accompanied with barrier breakdown including stroke,
362 multiple sclerosis, Alzheimer's diseases, and cerebral hemorrhage (Avolio et al., 2003; Kook et
363 al., 2013; Rosell et al., 2008; Underly et al., 2017). Given the ability of a single dose of rSPOCK1
364 to mitigate much of the leakage in the mutants and restore proper vascular expression of BBB

genes, we propose that Spock1 may serve as a new therapeutic target to reduce gelatinase activity in these neurological diseases and help restore barrier function.

Acknowledgments

We thank members of the Megason laboratory for data discussion and comments on the manuscript; Dr. Zach O'Brown for discussions and comments on the manuscript; Ignas Mazelis for single cell demultiplexing software; the HMS Single Cell Core for single cell library preparation; Dr. Bela Anand-Apte (Cleveland Clinic) for providing the transgenic *l-fabp:DBP-EGFP* fish line (Xie et al., 2010) and Dr. Leonard Zon for providing the transgenic Tg(*kdrl:HRAS-mCherry*) line; and the HMS Electron Microscopy Core Facility, with special thanks to Louise Trakimas for all of her assistance in preparing the TEM samples. This work was supported by the Damon Runyon Cancer Foundation (N.M.O.), NIH R01HD096755 (S.G.M), an Allen Distinguished Investigator Award (C.G.), NIH R35NS116820 (C.G), and partially supported by Faculty Scholar grant from the Howard Hughes Medical Institute (C.G.). C.G. is an investigator of the Howard Hughes Medical Institute.

Author Contributions

N.M.O., S.G.M. and C.G. conceived the project and designed experiments. N.M.O. performed all experiments and analyzed most data with the exception of the scRNA-seq which was performed in collaboration with and analyzed by N.B.P. and A.M.K. U.H. provided the *Spock1*$^{-/-}$ mice. N.M.O., S.G.M. and C.G wrote the manuscript.

References and Notes:

Abbott, N.J. (2004). Evidence for bulk flow of brain interstitial fluid: significance for physiology and pathology. Neurochem Int *45*, 545–552. https://doi.org/10.1016/j.neuint.2003.11.006.

Abbott, N.J., Rönnbäck, L., and Hansson, E. (2006). Astrocyte–endothelial interactions at the blood–brain barrier. Nature Reviews. Neuroscience *7*, 41–53. https://doi.org/10.1038/nrn1824.

Ando, K., Fukuhara, S., Izumi, N., Nakajima, H., Fukui, H., Kelsh, R.N., and Mochizuki, N. (2016). Clarification of mural cell coverage of vascular endothelial cells by live imaging of zebrafish. Development (Cambridge, England) *143*, 1328–1339. https://doi.org/10.1242/dev.132654.

Andreone, B.J., Chow, B.W., Tata, A., Lacoste, B., Ben-Zvi, A., Bullock, K., Deik, A.A., Ginty, D.D., Clish, C.B., and Gu, C. (2017). Blood-Brain Barrier Permeability Is Regulated by Lipid Transport-Dependent Suppression of Caveolae-Mediated Transcytosis. Neuron *94*, 581-594.e5. https://doi.org/10.1016/j.neuron.2017.03.043.

Armulik, A., Genové, G., Mäe, M., Nisancioglu, M.H., Wallgard, E., Niaudet, C., He, L., Norlin, J., Lindblom, P., Strittmatter, K., et al. (2010). Pericytes regulate the blood-brain barrier. Nature *468*, 557–561. https://doi.org/10.1038/nature09522.

Armulik, A., Genové, G., and Betsholtz, C. (2011). Pericytes: Developmental, Physiological, and Pathological Perspectives, Problems, and Promises. Developmental Cell *21*, 193–215. https://doi.org/10.1016/j.devcel.2011.07.001.

Avolio, C., Ruggieri, M., Giuliani, F., Liuzzi, G.M., Leante, R., Riccio, P., Livrea, P., and Trojano, M. (2003). Serum MMP-2 and MMP-9 are elevated in different multiple sclerosis subtypes. J Neuroimmunol *136*, 46–53. https://doi.org/10.1016/s0165-5728(03)00006-7.

Ayloo, S., Lazo, C.G., Sun, S., Zhang, W., Cui, B., and Gu, C. (2022). Pericyte-to-endothelial cell signaling via vitronectin-integrin regulates blood-CNS barrier. Neuron https://doi.org/10.1016/j.neuron.2022.02.017.

Bell, R.D., Winkler, E.A., Sagare, A.P., Singh, I., LaRue, B., Deane, R., and Zlokovic, B.V. (2010). Pericytes control key neurovascular functions and neuronal phenotype in the adult brain and during brain aging. Neuron *68*, 409–427. https://doi.org/10.1016/j.neuron.2010.09.043.

Benz, F., Wichitnaowarat, V., Lehmann, M., Germano, R.F., Mihova, D., Macas, J., Adams, R.H., Taketo, M.M., Plate, K.-H., Guérit, S., et al. (2019). Low wnt/β-catenin signaling determines leaky vessels in the subfornical organ and affects water homeostasis in mice. Elife *8*, e43818. https://doi.org/10.7554/elife.43818.

Ben-Zvi, A., Lacoste, B., Kur, E., Andreone, B.J., Mayshar, Y., Yan, H., and Gu, C. (2014). Mfsd2a is critical for the formation and function of the blood-brain barrier. Nature *509*, 507–511. https://doi.org/10.1038/nature13324.

Bonnet, F., Périn, J.P., Charbonnier, F., Camuzat, A., Roussel, G., Nussbaum, J.L., and Alliel, P.M. (1996). Structure and cellular distribution of mouse brain testican. Association with the postsynaptic area of hippocampus pyramidal cells. The Journal of Biological Chemistry *271*, 4373–4380. https://doi.org/10.1074/jbc.271.8.4373.

426 Bresciani, E., Broadbridge, E., and Liu, P.P. (2018). An efficient dissociation protocol for
427 generation of single cell suspension from zebrafish embryos and larvae. Methodsx *5*, 1287–
428 1290. https://doi.org/10.1016/j.mex.2018.10.009.

429 Campbell, M., Kiang, A.-S., Kenna, P.F., Kerskens, C., Blau, C., O'Dwyer, L., Tivnan, A., Kelly,
430 J.A., Brankin, B., Farrar, G.-J., et al. (2008). RNAi-mediated reversible opening of the blood-
431 brain barrier. The Journal of Gene Medicine *10*, 930–947. https://doi.org/10.1002/jgm.1211.

432 Charbonnier, F., Chanoine, C., Cifuentes-Diaz, C., Gallien, C.L., Rieger, F., Alliel, P.M., and
433 Périn, J.P. (2000). Expression of the proteoglycan SPOCK during mouse embryo development.
434 Mechanisms of Development *90*, 317–321. https://doi.org/10.1016/s0925-4773(99)00255-5.

435 Chen, J., Luo, Y., Hui, H., Cai, T., Huang, H., Yang, F., Feng, J., Zhang, J., and Yan, X. (2017).
436 CD146 coordinates brain endothelial cell–pericyte communication for blood–brain barrier
437 development. Proc National Acad Sci *114*, E7622–E7631.
438 https://doi.org/10.1073/pnas.1710848114.

439 Chi, N.C., Shaw, R.M., Val, S.D., Kang, G., Jan, L.Y., Black, B.L., and Stainier, D.Y.R. (2008).
440 Foxn4 directly regulates tbx2b expression and atrioventricular canal formation. Genes &
441 Development *22*, 734–739. https://doi.org/10.1101/gad.1629408.

442 Cho, C., Smallwood, P.M., and Nathans, J. (2017). Reck and Gpr124 Are Essential Receptor
443 Cofactors for Wnt7a/Wnt7b-Specific Signaling in Mammalian CNS Angiogenesis and Blood-
444 Brain Barrier Regulation. Neuron *95*, 1056-1073.e5.
445 https://doi.org/10.1016/j.neuron.2017.07.031.

446 Choi, H.M.T., Schwarzkopf, M., Fornace, M.E., Acharya, A., Artavanis, G., Stegmaier, J.,
447 Cunha, A., and Pierce, N.A. (2018). Third-generation in situ hybridization chain reaction:
448 multiplexed, quantitative, sensitive, versatile, robust. Development (Cambridge, England) *145*.
449 https://doi.org/10.1242/dev.165753.

450 Daneman, R., Agalliu, D., Zhou, L., Kuhnert, F., Kuo, C.J., and Barres, B.A. (2009). Wnt/beta-
451 catenin signaling is required for CNS, but not non-CNS, angiogenesis. Proceedings of the
452 National Academy of Sciences of the United States of America *106*, 641–646.
453 https://doi.org/10.1073/pnas.0805165106.

454 Daneman, R., Zhou, L., Kebede, A.A., and Barres, B.A. (2010). Pericytes are required for blood-
455 brain barrier integrity during embryogenesis. Nature *468*, 562–566.
456 https://doi.org/10.1038/nature09513.

457 Du, Z., Lin, Z., Wang, Z., Liu, D., Tian, D., and Xia, L. (2020). SPOCK1 overexpression induced
458 by platelet-derived growth factor-BB promotes hepatic stellate cell activation and liver fibrosis
459 through the integrin Î±5Î²1/PI3K/Akt signaling pathway. Laboratory Investigation 1–15.
460 https://doi.org/10.1038/s41374-020-0425-4.

461 Edgell, C.-J.S., BaSalamah, M.A., and Marr, H.S. (2004). Testican-1: a differentially expressed
462 proteoglycan with protease inhibiting activities. International Review of Cytology *236*, 101–122.
463 https://doi.org/10.1016/s0074-7696(04)36003-1.

464 Garcia-Alloza, M., Prada, C., Lattarulo, C., Fine, S., Borrelli, L.A., Betensky, R., Greenberg,
465 S.M., Frosch, M.P., and Bacskai, B.J. (2009). Matrix metalloproteinase inhibition reduces
466 oxidative stress associated with cerebral amyloid angiopathy in vivo in transgenic mice. J
467 Neurochem *109*, 1636–1647. https://doi.org/10.1111/j.1471-4159.2009.06096.x.

468 Guemez-Gamboa, A., Nguyen, L.N., Yang, H., Zaki, M.S., Kara, M., Ben-Omran, T., Akizu, N.,
469 Rosti, R.O., Rosti, B., Scott, E., et al. (2015). Inactivating mutations in MFSD2A, required for
470 omega-3 fatty acid transport in brain, cause a lethal microcephaly syndrome. Nature Genetics
471 *47*, 809–813. https://doi.org/10.1038/ng.3311.

472 Guérit, S., Fidan, E., Macas, J., Czupalla, C.J., Figueiredo, R., Vijikumar, A., Yalcin, B.H.,
473 Thom, S., Winter, P., Gerhardt, H., et al. (2021). Astrocyte-derived Wnt growth factors are
474 required for endothelial blood-brain barrier maintenance. Prog Neurobiol *199*, 101937.
475 https://doi.org/10.1016/j.pneurobio.2020.101937.

476 Hallmann, R., Mayer, D.N., Berg, E.L., Broermann, R., and Butcher, E.C. (1995). Novel mouse
477 endothelial cell surface marker is suppressed during differentiation of the blood brain barrier.
478 Dev Dynam *202*, 325–332. https://doi.org/10.1002/aja.1002020402.

479 Heithoff, B.P., George, K.K., Phares, A.N., Zuidhoek, I.A., Munoz-Ballester, C., and Robel, S.
480 (2021). Astrocytes are necessary for blood–brain barrier maintenance in the adult mouse brain.
481 Glia *69*, 436–472. https://doi.org/10.1002/glia.23908.

482 Henson, H.E., Parupalli, C., Ju, B., and Taylor, M.R. (2014). Functional and genetic analysis of
483 choroid plexus development in zebrafish. Frontiers in Neuroscience *8*, 364.
484 https://doi.org/10.3389/fnins.2014.00364.

485 Herrero-Navarro, Á., Puche-Aroca, L., Moreno-Juan, V., Sempere-Ferràndez, A., Espinosa, A.,
486 Susín, R., Torres-Masjoan, L., Leyva-Díaz, E., Karow, M., Figueres-Oñate, M., et al. (2021).
487 Astrocytes and neurons share region-specific transcriptional signatures that confer regional
488 identity to neuronal reprogramming. Sci Adv *7*, eabe8978.
489 https://doi.org/10.1126/sciadv.abe8978.

490 Janzer, R.C., and Raff, M.C. (1987). Astrocytes induce blood-brain barrier properties in
491 endothelial cells. Nature *325*, 253–257. https://doi.org/10.1038/325253a0.

492 Jeong, J.-Y., Kwon, H.-B., Ahn, J.-C., Kang, D., Kwon, S.-H., Park, J.A., and Kim, K.-W. (2008).
493 Functional and developmental analysis of the blood–brain barrier in zebrafish. Brain Research
494 Bulletin *75*, 619–628. https://doi.org/10.1016/j.brainresbull.2007.10.043.

495 Junge, H.J., Yang, S., Burton, J.B., Paes, K., Shu, X., French, D.M., Costa, M., Rice, D.S., and
496 Ye, W. (2009). TSPAN12 Regulates Retinal Vascular Development by Promoting Norrin- but
497 Not Wnt-Induced FZD4/β-Catenin Signaling. Cell *139*, 299–311.
498 https://doi.org/10.1016/j.cell.2009.07.048.

499 Klein, A.M., Mazutis, L., Akartuna, I., Tallapragada, N., Veres, A., Li, V., Peshkin, L., Weitz,
500 D.A., and Kirschner, M.W. (2015). Droplet Barcoding for Single-Cell Transcriptomics Applied to
501 Embryonic Stem Cells. Cell *161*, 1187–1201. https://doi.org/10.1016/j.cell.2015.04.044.

Kook, S.-Y., Hong, H.S., Moon, M., and Mook-Jung, I. (2013). Disruption of blood-brain barrier in Alzheimer disease pathogenesis. Tissue Barriers *1*, e23993. https://doi.org/10.4161/tisb.23993.

Li, B., and Dewey, C.N. (2011). RSEM: accurate transcript quantification from RNA-Seq data with or without a reference genome. BMC Bioinformatics *12*, 323. https://doi.org/10.1186/1471-2105-12-323.

Liebner, S., Corada, M., Bangsow, T., Babbage, J., Taddei, A., Czupalla, C.J., Reis, M., Felici, A., Wolburg, H., Fruttiger, M., et al. (2008). Wnt/β-catenin signaling controls development of the blood–brain barrier. J Cell Biology *183*, 409–417. https://doi.org/10.1083/jcb.200806024.

Lyck, R., Ruderisch, N., Moll, A.G., Steiner, O., Cohen, C.D., Engelhardt, B., Makrides, V., and Verrey, F. (2009). Culture-induced changes in blood-brain barrier transcriptome: implications for amino-acid transporters in vivo. Journal of Cerebral Blood Flow and Metabolism : Official Journal of the International Society of Cerebral Blood Flow and Metabolism *29*, 1491–1502. https://doi.org/10.1038/jcbfm.2009.72.

Martin, M., Vermeiren, S., Bostaille, N., Eubelen, M., Spitzer, D., Vermeersch, M., aci, C.P., Pozuelo, E., Toussay, X., Raman-Nair, J., et al. (2022). Engineered Wnt ligands enable blood-brain barrier repair in neurological disorders. Science *375*. https://doi.org/10.1126/science.abm4459.

McGinnis, C.S., Patterson, D.M., Winkler, J., Conrad, D.N., Hein, M.Y., Srivastava, V., Hu, J.L., Murrow, L.M., Weissman, J.S., Werb, Z., et al. (2019). MULTI-seq: sample multiplexing for single-cell RNA sequencing using lipid-tagged indices. Nat Methods *16*, 619–626. https://doi.org/10.1038/s41592-019-0433-8.

Miller, A.C., Obholzer, N.D., Shah, A.N., Megason, S.G., and Moens, C.B. (2013). RNA-seq-based mapping and candidate identification of mutations from forward genetic screens. Genome Research *23*, 679–686. https://doi.org/10.1101/gr.147322.112.

Nakada, M., Yamada, A., Takino, T., Miyamori, H., Takahashi, T., Yamashita, J., and Sato, H. (2001). Suppression of membrane-type 1 matrix metalloproteinase (MMP)-mediated MMP-2 activation and tumor invasion by testican 3 and its splicing variant gene product, N-Tes. Cancer Research *61*, 8896–8902. .

O'Brown, N.M., Megason, S.G., and Gu, C. (2019). Suppression of transcytosis regulates zebrafish blood-brain barrier function. ELife *8*, 41. https://doi.org/10.7554/elife.47326.

Ohlig, S., Clavreul, S., Thorwirth, M., Simon-Ebert, T., Bocchi, R., Ulbricht, S., Kannayian, N., Rossner, M., Sirko, S., Smialowski, P., et al. (2021). Molecular diversity of diencephalic astrocytes reveals adult astrogenesis regulated by Smad4. Embo J *40*, e107532. https://doi.org/10.15252/embj.2020107532.

Pomreinke, A.P., Soh, G.H., Rogers, K.W., Bergmann, J.K., Bläßle, A.J., and Müller, P. (2017). Dynamics of BMP signaling and distribution during zebrafish dorsal-ventral patterning. Elife *6*, e25861. https://doi.org/10.7554/elife.25861.

Raj, B., Farrell, J.A., Liu, J., Kholtei, J.E., Carte, A.N., Acedo, J.N., Du, L.Y., McKenna, A., Relić, Đ., Leslie, J.M., et al. (2020). Emergence of Neuronal Diversity during Vertebrate Brain Development. Neuron 1–24. https://doi.org/10.1016/j.neuron.2020.09.023.

Reese, T.S., and Karnovsky, M.J. (1967). Fine structural localization of a blood-brain barrier to exogenous peroxidase. J Cell Biology *34*, 207–217. https://doi.org/10.1083/jcb.34.1.207.

Röll, S., Seul, J., Paulsson, M., and Hartmann, U. (2006). Testican-1 is dispensable for mouse development. Matrix Biology *25*, 373–381. https://doi.org/10.1016/j.matbio.2006.05.004.

Rosell, A., Cuadrado, E., Ortega-Aznar, A., Hernández-Guillamon, M., Lo, E.H., and Montaner, J. (2008). MMP-9–Positive Neutrophil Infiltration Is Associated to Blood–Brain Barrier Breakdown and Basal Lamina Type IV Collagen Degradation During Hemorrhagic Transformation After Human Ischemic Stroke. Stroke *39*, 1121–1126. https://doi.org/10.1161/strokeaha.107.500868.

Sanchez-Covarrubias, L., Slosky, L.M., Thompson, B.J., Davis, T.P., and Ronaldson, P.T. (2014). Transporters at CNS barrier sites: obstacles or opportunities for drug delivery? Current Pharmaceutical Design *20*, 1422–1449. .

Stenman, J.M., Rajagopal, J., Carroll, T.J., Ishibashi, M., McMahon, J., and McMahon, A.P. (2008). Canonical Wnt Signaling Regulates Organ-Specific Assembly and Differentiation of CNS Vasculature. Science *322*, 1247–1250. https://doi.org/10.1126/science.1164594.

Stewart, P.A., and Wiley, M.J. (1981). Developing nervous tissue induces formation of blood-brain barrier characteristics in invading endothelial cells: A study using quail-chick transplantation chimeras. Dev Biol *84*, 183–192. https://doi.org/10.1016/0012-1606(81)90382-1.

Sweeney, M.D., Sagare, A.P., and Zlokovic, B.V. (2018). Blood–brain barrier breakdown in Alzheimer disease and other neurodegenerative disorders. Nature Publishing Group *14*, 133–150. https://doi.org/10.1038/nrneurol.2017.188.

Takahashi, Y., Maki, T., Liang, A.C., Itoh, K., Lok, J., Osumi, N., and Arai, K. (2014). p38 MAP kinase mediates transforming-growth factor-β1-induced upregulation of matrix metalloproteinase-9 but not -2 in human brain pericytes. Brain Res *1593*, 1–8. https://doi.org/10.1016/j.brainres.2014.10.029.

Traag, V.A., Waltman, L., and Eck, N.J. van (2019). From Louvain to Leiden: guaranteeing well-connected communities. Sci Rep-Uk *9*, 5233. https://doi.org/10.1038/s41598-019-41695-z.

Trost, A., Lange, S., Schroedl, F., Bruckner, D., Motloch, K.A., Bogner, B., Kaser-Eichberger, A., Strohmaier, C., Runge, C., Aigner, L., et al. (2016). Brain and Retinal Pericytes: Origin, Function and Role. Frontiers in Cellular Neuroscience *10*, 3171–13. https://doi.org/10.3389/fncel.2016.00020.

Umans, R.A., Henson, H.E., Mu, F., Parupalli, C., Ju, B., Peters, J.L., Lanham, K.A., Plavicki, J.S., and Taylor, M.R. (2017). CNS angiogenesis and barriergenesis occur simultaneously. Developmental Biology *425*, 101–108. https://doi.org/10.1016/j.ydbio.2017.03.017.

Underly, R.G., Levy, M., Hartmann, D.A., Grant, R.I., Watson, A.N., and Shih, A.Y. (2017). Pericytes as Inducers of Rapid, Matrix Metalloproteinase-9-Dependent Capillary Damage during Ischemia. The Journal of Neuroscience *37*, 129–140. https://doi.org/10.1523/jneurosci.2891-16.2016.

Urich, E., Lazic, S.E., Molnos, J., Wells, I., and Freskgård, P.-O. (2012). Transcriptional Profiling of Human Brain Endothelial Cells Reveals Key Properties Crucial for Predictive In Vitro Blood-Brain Barrier Models. PloS One *7*, e38149-16. https://doi.org/10.1371/journal.pone.0038149.

Váncza, L., Tátrai, P., Reszegi, A., Baghy, K., and Kovalszky, I. (2022). SPOCK1 with unexpected function. The start of a new career. Am J Physiol-Cell Ph https://doi.org/10.1152/ajpcell.00033.2022.

Vanhollebeke, B., Stone, O.A., Bostaille, N., Cho, C., Zhou, Y., Maquet, E., Gauquier, A., Cabochette, P., Fukuhara, S., Mochizuki, N., et al. (2015). Tip cell-specific requirement for an atypical Gpr124- and Reck-dependent Wnt/β-catenin pathway during brain angiogenesis. ELife *4*. https://doi.org/10.7554/elife.06489.

Wagner, D.E., Weinreb, C., Collins, Z.M., Briggs, J.A., Megason, S.G., and Klein, A.M. (2018). Single-cell mapping of gene expression landscapes and lineage in the zebrafish embryo. Science *108*, eaar4362-13. https://doi.org/10.1126/science.aar4362.

Wang, Y., Rattner, A., Zhou, Y., Williams, J., Smallwood, P.M., and Nathans, J. (2012). Norrin/Frizzled4 signaling in retinal vascular development and blood brain barrier plasticity. Cell *151*, 1332–1344. https://doi.org/10.1016/j.cell.2012.10.042.

Wang, Y., Pan, L., Moens, C.B., and Appel, B. (2013). Notch3 establishes brain vascular integrity by regulating pericyte number. Development (Cambridge, England) *141*, 307–317. https://doi.org/10.1242/dev.096107.

Wang, Y., Cho, C., Williams, J., Smallwood, P.M., Zhang, C., Junge, H.J., and Nathans, J. (2018). Interplay of the Norrin and Wnt7a/Wnt7b signaling systems in blood–brain barrier and blood–retina barrier development and maintenance. Proceedings of the National Academy of Sciences of the United States of America *115*, E11827–E11836. https://doi.org/10.1073/pnas.1813217115.

Weinreb, C., Wolock, S., and Klein, A.M. (2017). SPRING: a kinetic interface for visualizing high dimensional single-cell expression data. Bioinformatics *34*, 1246–1248. https://doi.org/10.1093/bioinformatics/btx792.

Westerfield, M. (1993). The zebrafish book: a guide for the laboratory use of zebrafish (Brachydanio rerio).

Wolburg, H., and Paulus, W. (2010). Choroid plexus: biology and pathology. Acta Neuropathologica *119*, 75–88. https://doi.org/10.1007/s00401-009-0627-8.

Xie, J., Farage, E., Sugimoto, M., and Anand-Apte, B. (2010). A novel transgenic zebrafish model for blood-brain and blood-retinal barrier development. BMC Developmental Biology *10*, 76. https://doi.org/10.1186/1471-213x-10-76.

615 Xu, Q., Wang, Y., Dabdoub, A., Smallwood, P.M., Williams, J., Woods, C., Kelley, M.W., Jiang,
616 L., Tasman, W., Zhang, K., et al. (2004). Vascular Development in the Retina and Inner Ear
617 Control by Norrin and Frizzled-4, a High-Affinity Ligand-Receptor Pair. Cell *116*, 883–895.
618 https://doi.org/10.1016/s0092-8674(04)00216-8.

619 Ye, Z., Chen, J., Hu, X., Yang, S., Xuan, Z., Lu, X., and Zhao, Q. (2020). SPOCK1: a multi-
620 domain proteoglycan at the crossroads of extracellular matrix remodeling and cancer
621 development. Am J Cancer Res *10*, 3127–3137. .

622 Zhou, Y., and Nathans, J. (2014). Gpr124 Controls CNS Angiogenesis and Blood-Brain Barrier
623 Integrity by Promoting Ligand-Specific Canonical Wnt Signaling. Dev Cell *31*, 248–256.
624 https://doi.org/10.1016/j.devcel.2014.08.018.

625 Zhou, Y., Wang, Y., Tischfield, M., Williams, J., Smallwood, P.M., Rattner, A., Taketo, M.M., and
626 Nathans, J. (2014). Canonical WNT signaling components in vascular development and barrier
627 formation. J Clin Invest *124*, 3825–3846. https://doi.org/10.1172/jci76431.

628 Zhu, Q., Shah, S., Dries, R., Cai, L., and Yuan, G.-C. (2018). Identification of spatially
629 associated subpopulations by combining scRNA-seq and sequential fluorescence in situ
630 hybridization data. Nat Biotechnol 10.1038/nbt.4260. https://doi.org/10.1038/nbt.4260.

631

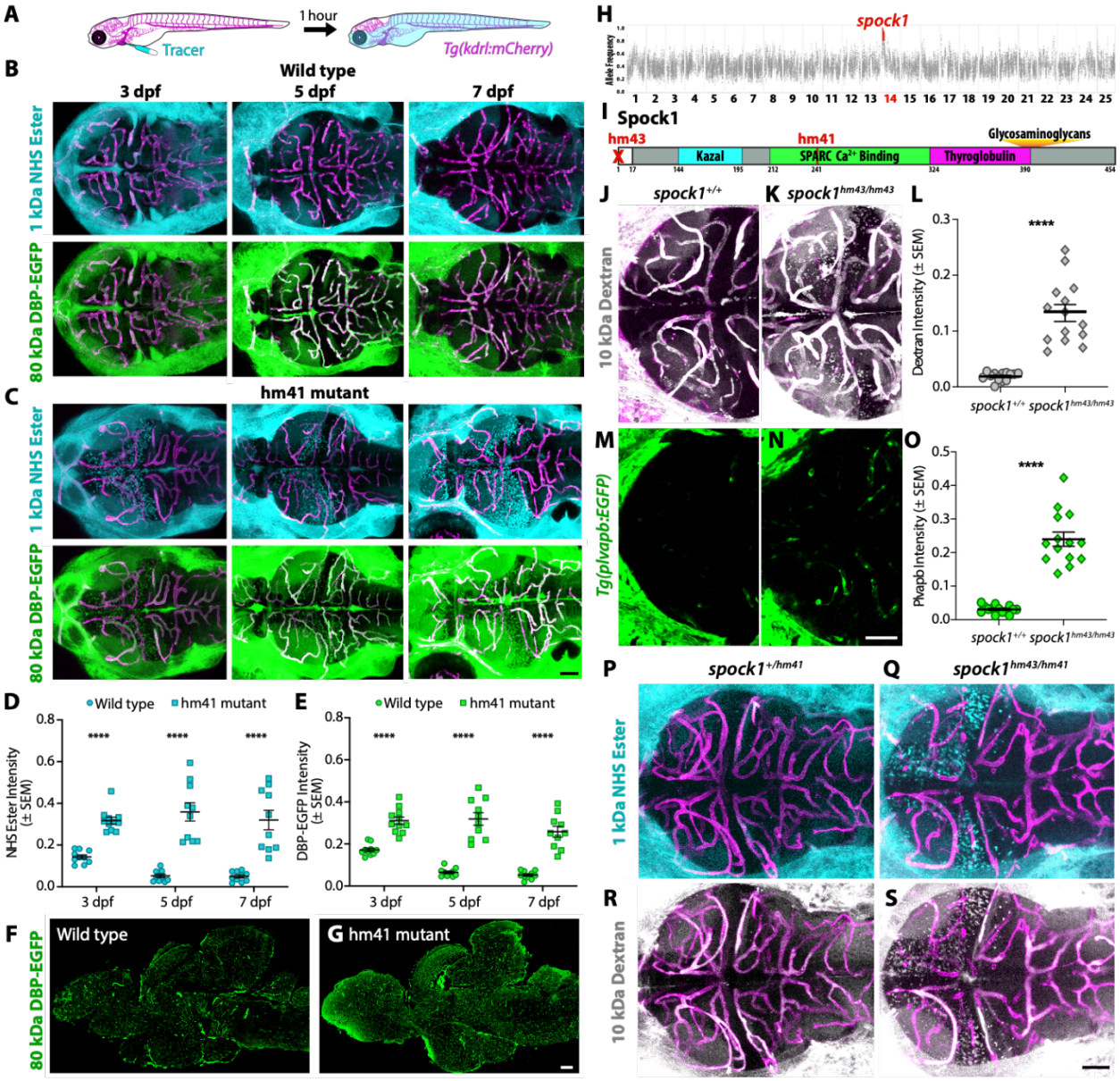

Figure 1. Spock1 induces BBB functional development.

(**A-E**) Fluorescent tracer leakage assays in larval zebrafish reveal BBB leakage in the forebrain and midbrain of both injected 1 kDa Alexa Fluor 405 NHS Ester (turquoise) and 80 kDa DBP-EGFP (green) of *hm41* homozygous larvae (C) compared to wild type controls (B) throughout larval development, as quantified in D and E. (**F-G**) Sagittal sections of adult brains show that the mutant leakage persists into adulthood (G). (**H**) Linkage mapping of the *hm41* mutant phenotype reveals tight linkage to *spock1* on chromosome 14. (**I**) *Spock1*^{hm41} has several point mutations (T241A and several silent mutations) in the SPARC domain. *Spock1*^{hm43} has a deletion of the 5' UTR and start codon. (**J-O**) Dextran leakage assays show *spock1*$^{hm43/hm43}$ mutants (K) have

642 increased BBB leakage (L). *spock1*$^{hm43/hm43}$ mutants have increased expression of the leaky
643 vessel marker plvapb (N and O). (**P-S**) Compound *spock1*$^{hm43/hm41}$ heterozygotes also display
644 increased NHS Ester (Q) and Dextran (S) leakage compared to *spock1*$^{hm41/+}$ heterozygote
645 siblings, which confine both injected tracers at 5 dpf (P and R). Scale bars represent 50 µm (C,
646 N, S) and 200 µm (G). **** $p<0.0001$ by 2way ANOVA (D and E) and by t test (L and O).

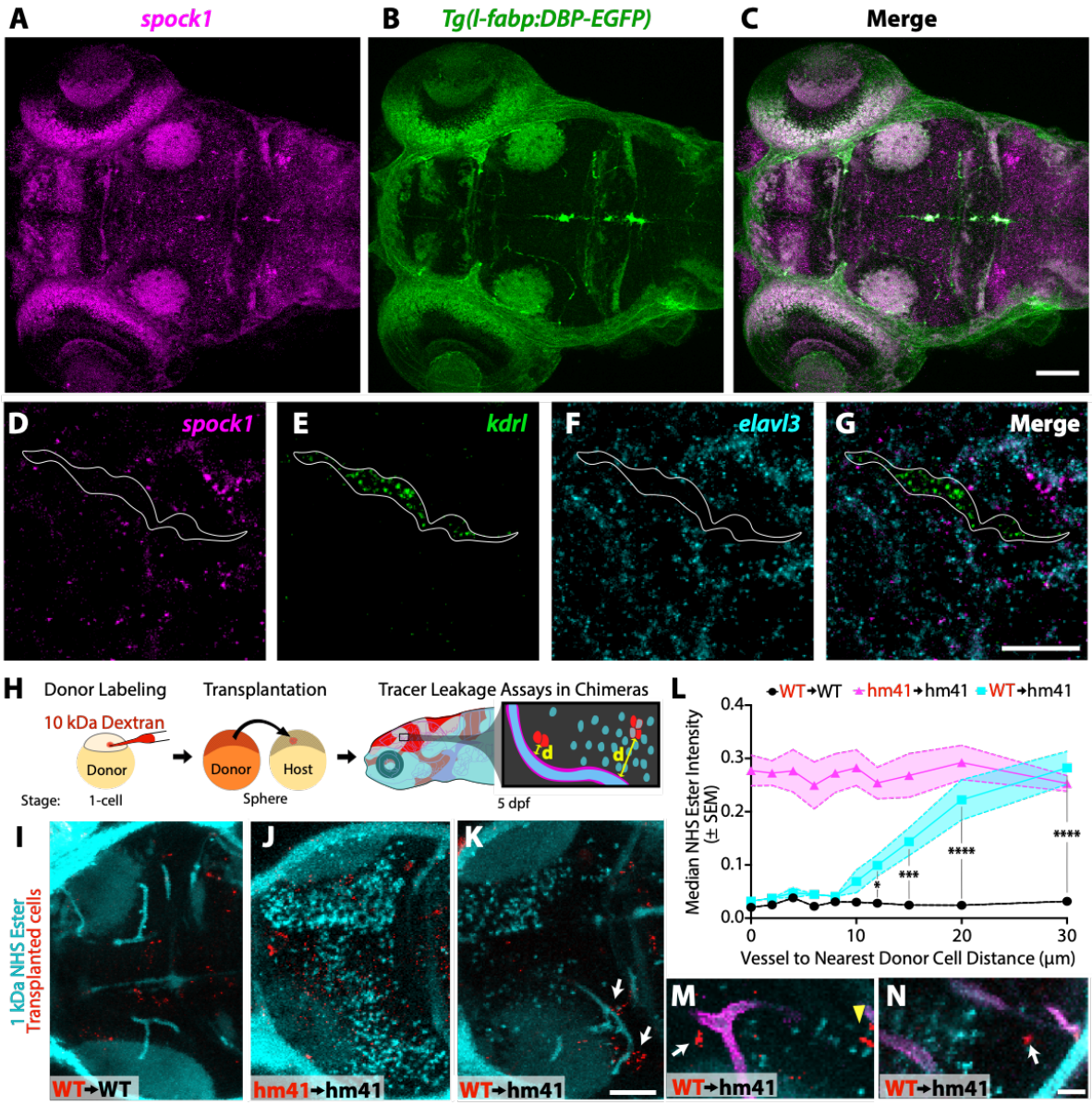

Figure 2. Neuronal Spock1 regulates endothelial cells within a 10-20 µm range. (**A-C**) Whole-mount HCR *in situ* hybridization for *spock1* (A) reveals signal throughout the entire 5 dpf brain, which is outlined by the fixed DBP-EGFP serum transgene (B). (**D-G**) Slide HCR *in situ* hybridization for *spock1* (D), the vascular transcript *kdrl* (E), and the neuronal transcript *elavl3* (F) reveal the lack of *spock1* signal in the vasculature (outlined in white). (**H**) Schematic of transplantation experiments. Cells from donor embryos labeled with 10 kDa Dextran (red) at the single cell stage are transplanted into unlabeled host embryos at sphere stage. Leakage of the injected 1 kDa AF 405 NHS Ester (turquoise) into the midbrain parenchyma is then measured in relationship to the distance (d) from the blood vessel to the nearest donor cell in the 5 dpf chimeric

657 larvae. (**I-K**) Representative dorsal 20 μm thick maximum intensity projection confocal image of a
658 chimeric larva with transplanted wild type donor cells (red) into a wild type host (I, WT→WT),
659 *spock1*$^{hm41/hm41}$ donor cells into a *spock1*$^{hm41/hm41}$ mutant host (J, hm41→hm41), and wild type
660 donor cells into a *spock1*$^{hm41/hm41}$ mutant host (K, WT→hm41). (**L**) Quantification of the NHS
661 leakage in WT→WT (black line) and hm41→hm41 (magenta line) reveals no change in tracer
662 leakage in relationship to the nearest donor cell, with wild type fish confining the tracer and mutant
663 fish leaking the tracer. However WT→hm41 (turquoise line) transplants reveal a full rescue of the
664 leakage in the mutant background when the transplanted cell is within 10 μm of a blood vessel
665 and no effect if the donor cell is further than 20 μm from the vessel. (**M-N**) Zoomed in images of
666 WT→hm41 transplants. The white arrows point to instances of local rescue of tracer (turquoise)
667 leakage when the wild type donor cell is close but not directly contacting the mutant vasculature
668 (magenta). The yellow arrowhead marks wild type donor cells that fall outside the range of
669 Spock1 signaling. Scale bars represent 50 μm (D and K) and 10 μm (G and N). * $p=0.0495$, ***
670 $p=0.0001$, **** $p<0.0001$ by 2way ANOVA compared to WT→WT transplants.
671

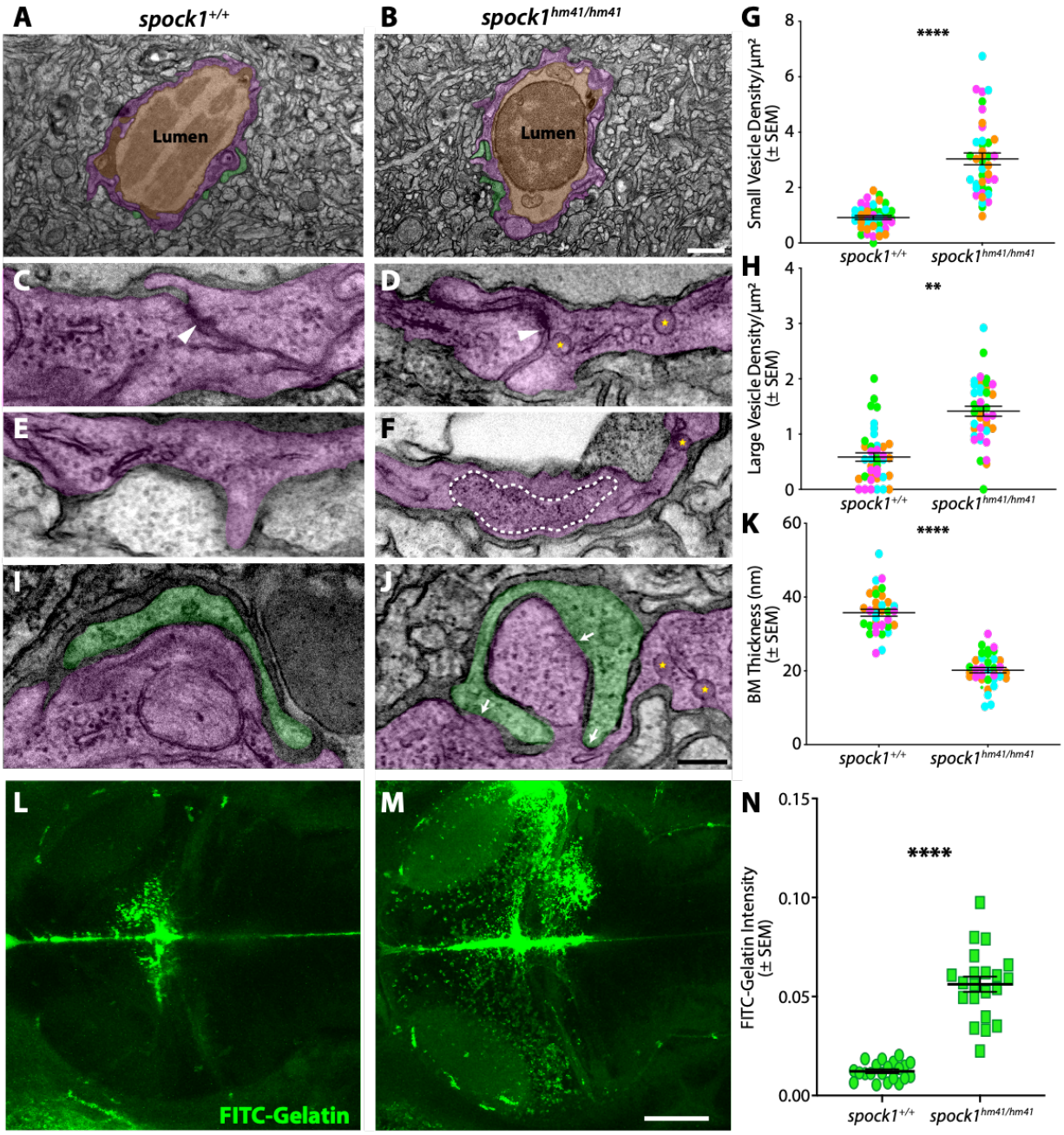

Figure 3. Spock1 mutants have increased endothelial vesicles. (**A-B**) The neurovascular unit remains intact in *spock1*$^{hm41/hm41}$ mutants (B) with a continuous single layer of endothelial cells (pseudocolored magenta) enclosing the lumen (pseudocolored orange) and in close contact with pericytes (pseudocolored green). (**C-H**) The majority of tight junctions (white arrowheads) are functionally restrictive in the *spock1*^{hm41} mutant endothelial cells (88%). Mutant endothelial cells displayed a significant increase in vesicular density, including both small flask shaped vesicles (yellow stars, G) and larger vesicles greater than 200 nm in diameter (outlined by white dashed

680 line in F, H). (**I-K**) While pericyte coverage is unaltered in *spock1*^{hm41} mutants, the pericyte-
681 endothelial cell interactions are altered in the mutants, with several instances of direct pericyte-
682 endothelial cell contact (white arrows) and overall diminished average basement membrane
683 thickness between the two vascular cells (K). (**L-N**) In vivo gelatin zymography in wild type (L)
684 and *spock1*$^{hm41/hm41}$ mutants (M) reveals significantly increased gelatinase activity in the mutant
685 midbrain compared to wild type siblings (N). Scale bars represent 1 μm (B), 200 nm (J), and 50
686 μm (M). ** $p=0.0029$ (H), **** $p<0.0001$ by nested t test (G and K) and by t test (N).

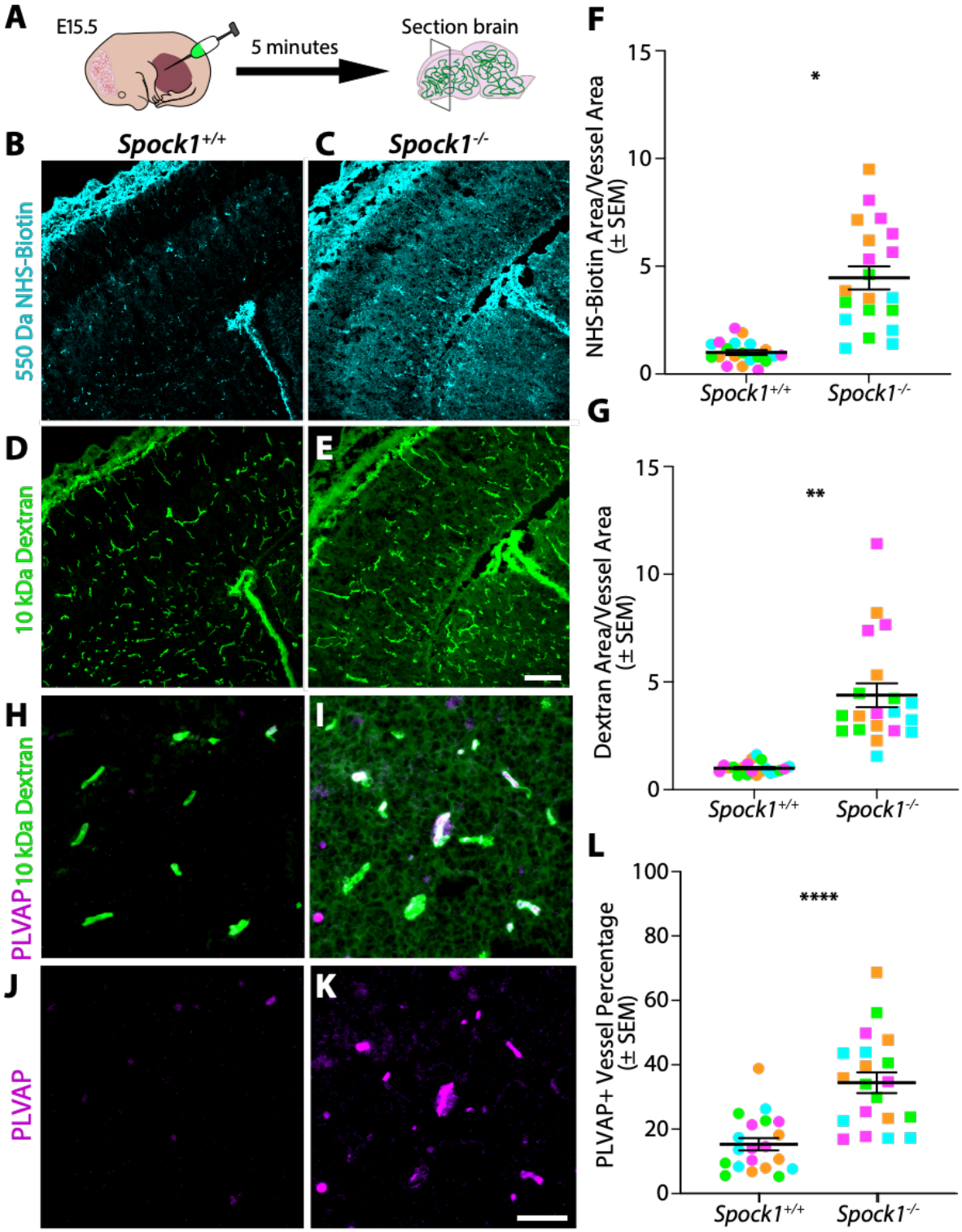

Figure 4. Spock1 plays a conserved role in inducing barrier function during embryonic development in mice. (A) Schematic of functional tracer leakage assays in embryonic day 15.5

690 (E15.5) mice. (**B-E**) Wild type mice confine both injected 550 Da NHS-Biotin (**B**) and 10 kDa
691 Dextran (**D**) within the vasculature, as previously reported. However, *Spock1*$^{-/-}$ mice leak both
692 NHS-Biotin (**C**) and Dextran (**E**) into the brain parenchyma. (**F-G**) Quantification of the total area
693 of NHS-Biotin leakage (F) and Dextran leakage (G) normalized to vessel area where a ratio of 1
694 indicates no leakage reveals a significant increase in extravasation of both tracers in the *Spock1*$^{-}$
695 $^{/-}$ embryos (p=0.0213 (F) and p=0.0048 (G) by nested t test). (**H-K**) Zoomed in view of 10 kDa
696 Dextran (green) confined within the vasculature of wild type (H) vessels and leaked out into the
697 cortex of *Spock1*$^{-/-}$ knockouts (I). This increased BBB permeability in *Spock1*$^{-/-}$ mice is
698 accompanied by an increase in PLVAP (magenta) expression in the vasculature (K). (**L**)
699 Quantification of PLVAP expression within the vasculature reveals a significant increase in
700 PLVAP expression in the *Spock1*$^{-/-}$ embryos (p<0.0001 by nested t test). N=4 embryos for each
701 genotype, marked by unique colors, with 5 sections analyzed per embryo. Scale bars represent
702 100 μm (E) and 50 μm (I).

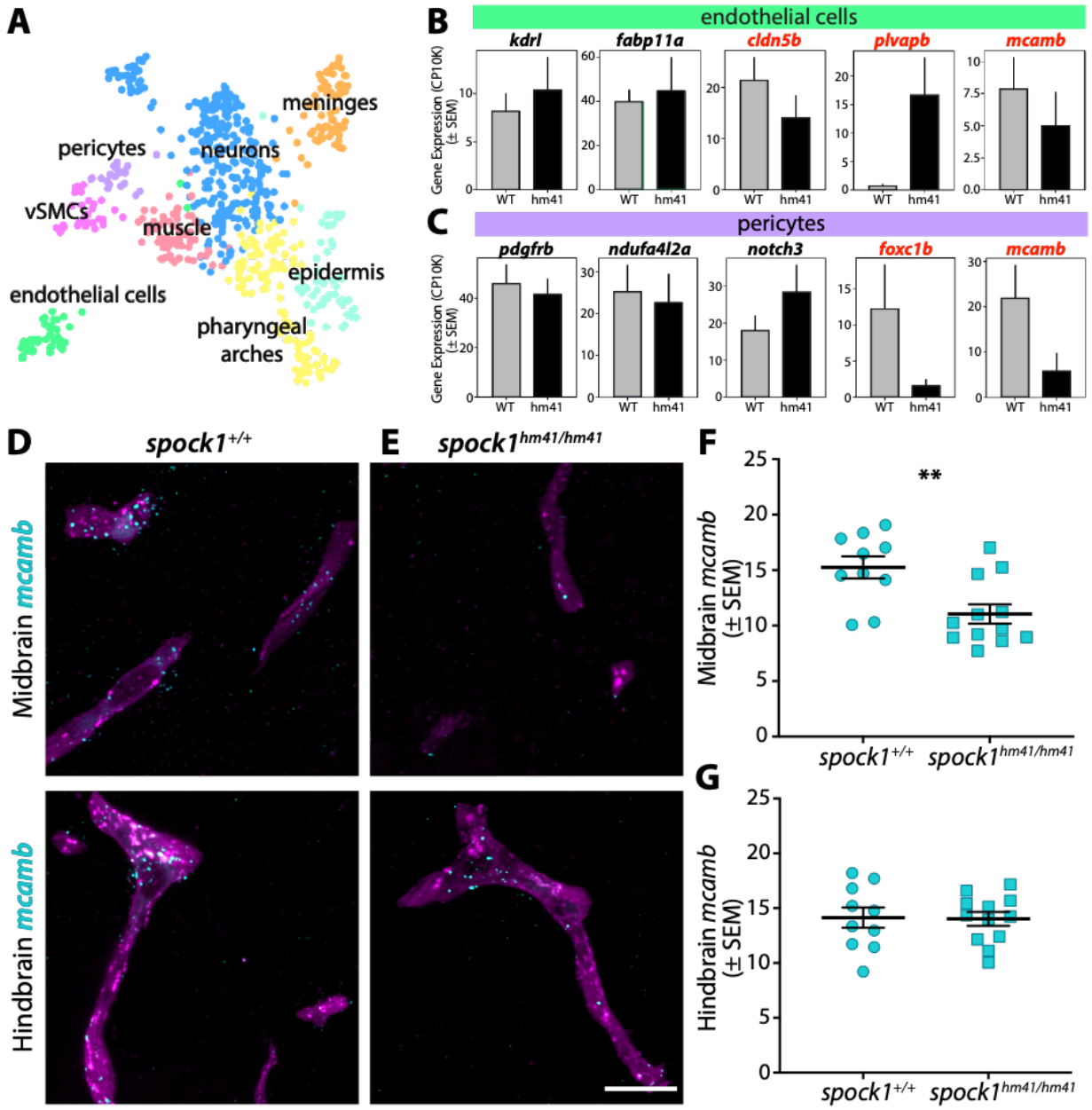

Figure 5. *Spock1*$^{hm41/hm41}$ mutant vascular cells have reduced expression of BBB regulators. (**A**) UMAP of the subclustered vascular cells separated by cell type, with pericytes (purple) separating from vascular smooth muscle cells (vSMCs, pink) and endothelial cells (green). (**B-C**) Mean gene expression in wild type (WT, grey bars) and *spock1* mutant (hm41, black bars) endothelial cells (B) and pericytes (C). Error bars represent SEM. Mutants appear to have lower levels of *mcamb* in both pericytes and endothelial cells. (**D-G**) HCR FISH reveals strong expression of *mcamb* (turquoise) in wild type vasculature (magenta) (D), both in the midbrain and hindbrain. *Spock1* mutants have significantly reduced expression of *mcamb* in the

712 midbrain (E, F), but normal levels in the hindbrain (G), where no leakage is observed. Scale bar
713 represents 10 μm. ** $p=0.0044$, **** $p<0.0001$ by unpaired t test.

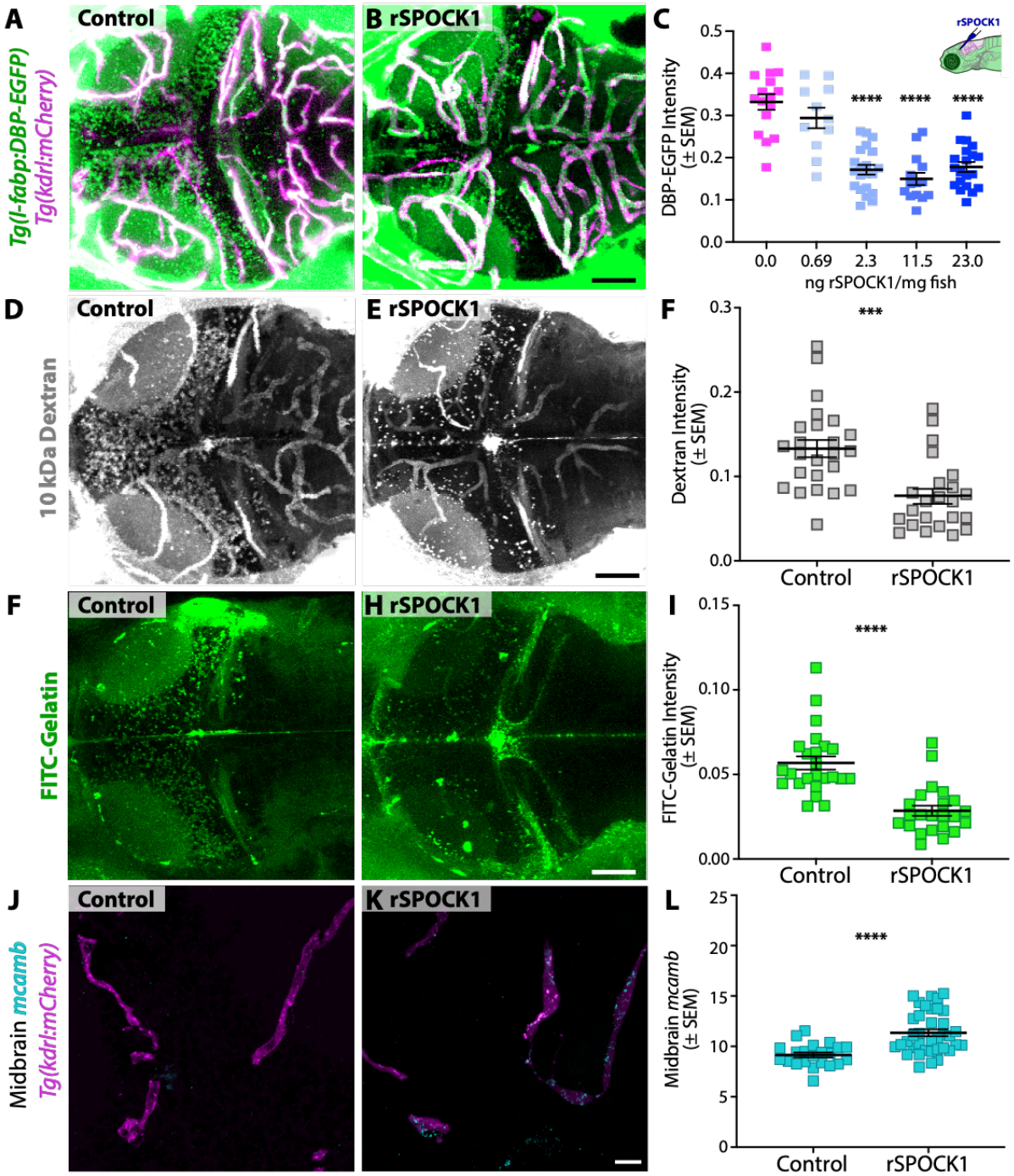

714

715 **Figure 6. Spock1 induces BBB properties by modulating the brain microenvironment,**
716 **altering vascular cell biology non-autonomously.** (**A-C**) A single intracranial injection of
717 human rSPOCK1 into the brain at 5 dpf reduces mutant leakage of DBP-EGFP at 6 dpf about
718 50% (B) compared to controls injected with PBS alone (A), quantified in C. (**D-F**) Similarly,
719 injection of rSPOCK1 at 4 dpf reduces mutant leakage of 10 kDa Dextran at 5 dpf (E), quantified

720 in F. (**F-I**) The addition of rSPOCK1 reduces gelatinase activity in the mutant brain (H) compared
721 to control injected mutants (F), quantified in I. (**J-L**) Vascular expression of *mcamb* in the midbrain
722 is partially restored following rSPOCK1 intracranial injections (K), quantified in L. Scale bars
723 represent 50 µm (C, E, F) and 10 µm (K). **** $p<0.0001$ by 2way ANOVA compared to PBS
724 injected control *spock1*$^{hm41/hm41}$ mutants in C and by t test in I and L, *** $p<0.001$ by t test in F.
725

726 **Supplementary Materials:**

727

728 **Materials and Methods**

729

730 **Zebrafish Strains and Maintenance**

731 Zebrafish were maintained at 28.5°C following standard protocols(Westerfield, 1993). All
732 zebrafish work was approved by the Harvard Medical Area Standing Committee on Animals under
733 protocol number IS00001263-3. Adult fish were maintained on a standard light-dark cycle from 8
734 am to 11 pm. Adult fish, age 3 months to 2 years, were crossed to produce embryos and larvae.
735 For imaging live larvae, 0.003% phenylthiourea (PTU) was used beginning at 1 dpf to inhibit
736 melanin production. These studies used the AB wild-type strains and the transgenic reporter
737 strains Tg(*l-fabp:DBP-EGFP)*^{lri500} (Xie et al., 2010), (Tg(*kdrl:HRAS-mCherry*)^{s896} (Chi et al., 2008),
738 abbreviated as Tg(*kdrl:mCherry*) in the text, TgBAC(*pdgfrb:EGFP)*^{ncv22Tg} (Ando et al., 2016),
739 abbreviated as Tg(*pdgfrb:EGFP*), and Tg(*plvapb:EGFP*)^{sj3Tg} (Umans et al., 2017), abbreviated
740 as Tg(*plvapb:EGFP*) in the text.

741

742 ***Spock1^{hm41}* Mutants**

743 *Spock1^{hm41}* mutants were maintained in the double transgenic Tg(*l-fabp:DBP-EGFP;*
744 *kdrl:mCherry)* background. Heterozygous fish were intercrossed for all leakage assays, with the
745 exception of the time lapse microscopy experiments, where a heterozygous fish was crossed to
746 a homozygous mutant, and the cell transplantation experiments, where homozygous mutants
747 were in-crossed. All larvae were imaged prior to genotyping to identify wild type and mutant fish.
748 The *spock1^{hm41}* mutant line was genotyped using 5'-ACTGAGTGTTATTTTGTCATTGTGC-3' and
749 5'-TGATGCTGATCTGAGAAGTTTAGCC-3' primers followed by a HaeIII restriction digest, which
750 does not digest the wild-type product (327 bp).

751

752 ***Spock1^{hm43}* Mutants**

753 *Spock1^{hm43}* mutants were generated and maintained in the double transgenic Tg(*plvap:EGFP;*
754 *kdrl:mCherry)* background using CRISPR mutagenesis with two sgRNAs (5'-
755 GTTCGTCACTTTAAAAGGAG-3' and 5'-TCTCAGATGATGTTGAGTCT-3') to target the *spock1*
756 5' UTR and start codon. Heterozygous fish were intercrossed for all leakage assays. All larvae
757 were imaged prior to genotyping to identify wild type and mutant fish. The *spock1^{hm43}* mutant line
758 was genotyped using 5'-TAAACTTCGATTGTGCTTTGGTTT G-3' and 5'-
759 AATGACTACAGACCTTTGAGGGAAC-3' primers and KAPA HiFi Hotstart polymerase

760 (Roche:KK2602) using a 58°C melting temperature. The mutant PCR product of 364 bp was
761 easily distinguishable by gel electrophoresis from the wild type product at 935 bp.
762
763 **Fluorescent Zebrafish Tracer Injections and Live Imaging**
764 Larvae were immobilized with tricaine and placed in an agarose injection mold with their hearts
765 facing upwards. 2.3 nl of Alexa Fluor 405 NHS Ester (Thermo Fisher: A30000) or Alexa Fluor 647
766 10 kDa Dextran (Thermo Fisher: D22914) fluorescently conjugated tracers (10 mg/ml) were
767 injected into the cardiac sac using Nanoject II (Drummond Scientific, Broomall, PA). Larvae were
768 then mounted with 1.5% low gelling agarose (Sigma: A9414) in embryo water on 0.17 mm
769 coverslips and imaged live within 2 hours post injection on a Leica SP8 laser scanning confocal
770 microscope using the same acquisition settings with 1 µm z-steps using a 25x water immersion
771 objective. All quantification was performed on blinded image sets. For static images, parenchymal
772 fluorescent tracer intensity was measured using ImageJ in the entire regional parenchyma outside
773 of the vasculature in 60 µm thick maximum intensity projections of the larval brains. These
774 projections began on average 15 µm below the mesencephalic vein to reduce the effects of
775 potential leakage diffusion from the surface vessels and had the vasculature masked and
776 removed for intensity quantification. These parenchymal tracer intensity values were then
777 background subtracted and normalized to the tracer intensity within the vasculature to account
778 for differential amounts of circulating tracer between fish. For time lapse imaging, Dextran
779 intensity was measured in six parenchymal regions of average intensity projections of the time
780 lapse videos and averaged as a single value per fish and similarly normalized to the average
781 blood vessel luminal fluorescence intensity at each time point. Pericyte and vascular double
782 transgenics were similarly imaged on the Leica SP8 for quantification of vascular defects.
783 Additional images were taken on a Zeiss LSM 980 with Airyscan 2 with 0.21 µm z-steps using a
784 20x water immersion objective for increased cellular resolution, allowing us to detect gaps
785 between the two cell types in vivo.
786
787 **Linkage Mapping**
788 Larvae from 2 separate crosses were screened for leakage of DBP-EGFP at 5 dpf and pooled
789 into 3 groups of 5 to 6 leaky or wild type heads. RNA was extracted from the pools using RNeasy
790 mini kit and ribo-depleted. RNA sequencing libraries were prepared using Wafergen Directional
791 RNA-Seq kits and sequenced on NextSeq High-Output sequencers producing 75 bp paired end
792 reads. Reads were mapped to the GRCz11 genome using tophat and bowtie2. Linkage mapping
793 was performed on the mapped reads using RNAmapper(Miller et al., 2013) with the following

794 specifications: zygosity=25, coverage=1, linkedRatio=0.96, neighbors=10. Differential gene
795 expression analysis was performed on these libraries using rsem(Li and Dewey, 2011).
796
797 **CRISPR Mutants**
798 *Gstp2* crispant fish were generated by injection of Cas9 protein and 3 guide RNAs (5'-
799 CAGCTGCCTAAATTTGAAGA-3', 5'-GCGTTGGAAACTTACACATG-3', and 5'-GTGAG
800 AGTGTAGGGAGCCAC-3') into 1-cell fertilized double transgenic Tg(*l-fabp:DBP-EGFP;*
801 *kdrl:mCherry)* embryos. *Csf1ra* crispant fish were generated similarly with 4 guide RNAs (5'-
802 CTGCTCACCAACAGCCGAG-3', 5'-GTGTCTTCTGACCGACCCGG-3', 5'-CTCGTC
803 TTCATGCTTCACG-3', and 5'-AGTGACACCTTCTCCATGG-3'), as were *spock1* crispants (5'-
804 GTAGCCGACAGAAAGAGAGG-3', 5'-GAGTCGCAGGAGTTGAACAG-3', 5'-
805 GACAGTGAACCTTCATGCAG-3', and 5'-TGTCCGGGCAGGCAAGGGCA-3'). F0 crispants
806 were analyzed for leakage of the DBP-EGFP tracer outside of the kdrl:mCherry labeled
807 vasculature at 5 dpf.
808
809 **HCR Fluorescent In Situ Hybridization (FISH)**
810 *Slide*: HCR RNA in situ hybridization (Molecular Instruments) experiments on 14 µm cryosections
811 of fixed 5 dpf larvae were performed as previously described (Choi et al., 2018; O'Brown et al.,
812 2019). Briefly, sections were air dried and re-fixed in 4% paraformaldehyde (PFA) in PBS for 10
813 minutes at room temperature. Following fixation, slides were washed in PBS and then
814 permeabilized using 1 µg/ml Proteinase K (ThermoFisher) for 5 minutes, followed by PBS washes
815 and refixation. Tissues were further permeabilized by an ethanol dehydration series of 50%, 70%
816 and two rounds of 100% ethanol and air dried for 5 minutes. Dried slides were put into probe
817 hybridization solution for at least 10 minutes at 37°C. Subsequently, the probes for *spock1, kdrl,*
818 *elavl3,* and *mcamb* were added to the slides at a final concentration of 4 nM to hybridize overnight
819 at 37°C. The next day, slides were washed with a series of wash buffer to 5x SSCT (5x SSC with
820 0.1% Tween 20). Excess liquid was then removed and samples were immersed in amplification
821 buffer at room temperature for 30 minutes prior to hairpin amplification, which occurred overnight
822 at room temperature. Slides were then washed in 5x SSCT, washed in 5x SSC and mounted with
823 Fluoromount-G (Electron Microscopy Sciences).
824
825 *Whole mount*: Larvae were fixed in 4% PFA overnight and then stored in methanol at -20°C until
826 staining was performed. All staining was performed in PCR strip tubes. Larvae were rehydrated
827 in a series of methanol/PBST (0.1% Tween) washes and then permeabilized with 30 µg/ml

828 Proteinase K for 45 minutes at room temperature. Larvae were then refixed in 4% PFA for 20
829 minutes and treated with probe hybridization buffer at 37°C. Subsequently, the *spock1* probe was
830 added at a final concentration of 4 nM to hybridize overnight rocking at 37°C. The next day, larvae
831 were washed with a series of wash buffer to 5x SSCT (5x SSC with 0.1% Tween 20). Excess
832 liquid was then removed and samples were immersed in amplification buffer at room temperature
833 for 30 minutes prior to hairpin amplification, which occurred overnight rocking at room
834 temperature. Larvae were then washed and imaged in 5x SSCT.
835
836 Images for quantification were collected on a Leica SP8 laser scanning confocal microscope using
837 the same acquisition settings with 0.2 µm z-steps using a 25x water immersion objective or a 63x
838 oil immersion lens. All quantification was performed on blinded image sets of sections from a
839 single slide treated with all of the same reagents and imaged on the same day. To measure levels
840 of *mcamb* expression, we used ImageJ to first subtract tissue autofluorescence (captured in the
841 405 channel) from the *mcamb* expression in maximum intensity projections and then the
842 vasculature was manually traced and average intensity was measured. Additional images were
843 taken on a Zeiss LSM 980 with Airyscan 2 with 0.21 µm z-steps using either a 20x or a 40x water
844 immersion objective to further enhance the resolution of the *mcamb* signal.
845
846 **Transplantation**
847 Donor embryos were injected with 2.3 nl of 10 mg/ml Alexa Fluor 647 10 kDa Dextran (Thermo
848 Fisher: D22914) at the 1-cell stage to distinguish them from host cells. Following injection,
849 embryos were incubated at 28.5°C until transplantation. Host and donor embryos were
850 dechorinated with 1 mg/ml Pronase (Roche:11459643001) at oblong stage and transferred to
851 transplantation agarose dishes in 1/3 Ringer's buffer. Unfertilized or injured embryos were
852 discarded. To generate clonal sources secreting wild type or mutant Spock1, approximately 40–
853 80 cells were transplanted from sphere stage dextran labeled donor embryos into sphere stage
854 wild type and mutant hosts (similar to previous studies(Pomreinke et al., 2017)). Embryos
855 recovered overnight in 1/3 Ringer's buffer and were subsequently transferred to Danieau Buffer
856 with PTU. Tracer injections were performed at 5 dpf, as described above, with 1 kDa Alexa Flour
857 405 NHS Ester. Blinded image sets were analyzed using ImageJ. Individual larval brains were
858 segmented into 10 µm thick maximum intensity projections spanning the entire brain. Average
859 NHS tracer intensity was measured in 10 µm wide swaths connecting donor cells to the nearest
860 blood vessel and normalized to average blood vessel tracer intensity. The median tracer intensity
861 for a given distance (D) to the nearest donor cell was calculated for each individual fish.

862

863 **Transmission Electron Microscopy (TEM)**

864 Larvae (7 dpf) were anesthetized with tricaine and injected with 2.3 nl of 5 nm NHS-activated gold
865 nanoparticles (Cytodiagnostics: CGN5K-5-1, ~1.1^{14} particles/ml in PBS) just as for the fluorescent
866 tracer injections. After 5 minutes of circulation, the larvae were initially fixed by immersion in 4%
867 paraformaldehyde (VWR:15713-S) /0.1M sodium-cacodylate (VWR:11653). Following this initial
868 fixation, larvae were further fixed for 7 days in 2% glutaraldehyde (Electron Microscopy Sciences:
869 16320)/ 4% paraformaldehyde/ 0.1M sodium-cacodylate at room temperature. Following fixation,
870 larvae were washed overnight in 0.1M sodium-cacodylate. Entire larval heads were post-fixed in
871 1% osmium tetroxide and 1.5% potassium ferrocyanide, dehydrated, and embedded in epoxy
872 resin. Ultrathin sections of 80 nm were then cut from the block surface and collected on copper
873 grids. Grids were imaged using a 1200EX electron microscope (JEOL) equipped with a 2k CCD
874 digital camera (AMT) and quantified using ImageJ (NIH). Vesicular density values were
875 calculated from the number of non-clathrin coated small vesicles less than 100 nm in diameter or
876 large vesicles greater than 200 nm in diameter per μm^2 of endothelial area for each image
877 collected. Average pericyte basement membrane (BM) thickness was quantified by measuring
878 the total BM area divided by the length of the pericyte-endothelial contact. All images for analysis
879 were collected at 12000x magnification. 10-15 vessels were quantified for each fish, with each
880 color representing a different fish.

881

882 **Intracranial rSPOCK1 Injections**

883 Larvae were anesthetized with tricaine and placed in an agarose injection mold with their heads
884 facing upwards. 2.3 nl of recombinant human SPOCK1 (rSPOCK1; R&D Systems: 2327-PI-050)
885 at a range of 0.001-10 mg/ml was injected directly into the midbrain using Nanoject II
886 (Drummond Scientific, Broomall, PA). Following injections, larvae recovered in normal embryo
887 water for 1 day. The effects of rSPOCK1 were either assess in live fish using functional tracer
888 leakage assays and in vivo gelatin zymography or in fixed samples followed by slide HCR in situ
889 hybridization, as described above.

890

891 **In vivo Gelatinase Zymography**

892 Larvae were anesthetized and intracranially injected as for rSPOCK1 with 2.3 nl of FITC-Gelatin
893 (Biovision: M1303) at 5 mg/ml. After one hour, larvae were also injected with 10 kDa Dextran in
894 the cardiac sac to assess BBB function and then mounted with 1.5% low gelling agarose (Sigma:
895 A9414) in embryo water on 0.17 mm coverslips and imaged live within 2 hours post injection on

896 a Leica SP8 laser scanning confocal microscope using the same acquisition settings with 1 μm
897 z-steps using a 25x water immersion objective. All quantification was performed on blinded image
898 sets. Parenchymal FITC-Gelatin probe intensity was measured using ImageJ in the entire
899 midbrain and normalized to the average intensity in the ventricles, which have high gelatinase
900 activity, to account for fish to fish injection variation. Regions of obvious damage at the injection
901 site were not quantified.
902
903 **Mouse Maintenance**
904 *Spock1*$^{-/-}$ knockout mice (Röll et al., 2006) were obtained from Ursula Hartmann's lab and were
905 backcrossed to and maintained on a C57Bl/6 background. Mice were genotyped with primers 5'-
906 GCCACTGGTCATTGTCTAGG-3', 5'- TGTGCCCAGTCATAGCCGAATAGC CTCTCC-3', and 5'-
907 GCTTGAGGTAGCCCTGTTGTCACC-3' using KAPA HiFi Hotstart polymerase (Roche:KK2602).
908 This PCR reaction produced a 185 bp wild type band and a 750 bp knockout band in heterozygous
909 animals. All animals were treated according to institutional and US National Institutes of Health
910 (NIH) guidelines approved by the Institutional Animal Care and Use Committee (IACUC) at
911 Harvard Medical School under protocol IS00000045-6.
912
913 **Mouse Tracer Injections**
914 Heterozygous *Spock1*$^{+/-}$ mice were intercrossed and used for tracer leakage assays performed at
915 embryonic day 15.5 (E15.5) as previously described(Ben-Zvi et al., 2014). In brief, 5 μl of tracer
916 cocktail (10 mg/ml EZ-Link NHS-Biotin (Thermo Fisher: 20217) and 5 mg/ml 10 kDa Dextran
917 Alexa Fluor 488 (Thermo Fisher: D22910)) was injected into the liver of each embryo and allowed
918 to circulate for 5 minutes. Embryonic heads were fixed by immersion in 4% paraformaldehyde
919 overnight at 4°C and then frozen in TissueTek OCT (Sakura). 20 μm thick sections were then
920 collected and immunostained with Streptavidin Alexa Fluor 405 (1:200; Thermo Fisher: S32351)
921 and rat anti-PLVAP (1:200; BD Biosciences:553849). All embryos were injected and fixed for
922 processing blind before genotyping. Adult mice were retroorbitally injected with 0.5 mg of EZ-Link
923 NHS-Biotin per g of mouse body weight. The NHS-Biotin circulated for 30 minutes prior to brain
924 dissections and fixation with 4% PFA. 30 μm thick cryosections were then collected and
925 immunostained with Streptavidin Alexa Fluor 568 (1:200; Thermo Fisher: S32351) and goat anti-
926 CD31 (1:100; R&D Systems: AF3628).
927
928 **Single-cell RNA-sequencing**

929 Larval zebrafish brains were dissected and split along the midbrain-hindbrain boundary in DMEM.
930 Brains were dissociated using a modified protocol(Bresciani et al., 2018). Briefly, chemical
931 dissociations were performed at 30.5°C using a mixture of 0.25% Trypsin-EDTA,
932 Collagenase/Dispase (8 mg/mL) and DNaseI (20 µg/mL) for 15-20 minutes with gentle pipetting
933 every few minutes and quenched with 10% fetal bovine serum in DMEM. Samples were hashed
934 using Multi-seq as previously described with slight modifications(McGinnis et al., 2019). For each
935 sample, 80 pmoles of lipid modified oligos (LMOs) were used to hash every 500k cells. The
936 hashing reaction was quenched using 1% BSA in PBS and barcoded samples were subsequently
937 pooled and washed with 1% BSA. The pooled cell mixture was resuspended in PBS + 0.1%BSA
938 + 18% Optiprep at a final concentration of ~300k cells/mL prior to single-cell capture with inDrops.
939 The Single-cell Core (SCC) at Harvard Medical School captured single-cell transcriptomes and
940 prepared NGS libraries as previously described(Klein et al., 2015) with a target capture of 45k
941 cells per experiment. A summary of dissected tissues and corresponding sequencing information
942 are described in Table S4.
943
944 Gene expression and hashtag libraries were mixed (9:1 ratio) and sequenced on an Illumina
945 Nova-seq 6000 with the NovaSeq S2 kit. Reads were mapped onto the Zebrafish GRCz11
946 Release 101 genome assembly using previously described methods(Wagner et al., 2018).
947 Hashtags were identified using custom code available on:
948 https://github.com/AllonKleinLab/paper-data/tree/master/OBrown2021_ZebrafishBBB
949
950 Transcriptomes with greater than 350 UMIs were further filtered for viability by removing cells with
951 >20% mitochondrial reads. Cell demultiplexing was performed manually by applying thresholds
952 to delineate single cells from background and multiple populations. The resulting counts matrix
953 was normalized to the mean UMIs per cell in the dataset.
954
955 To visualize the data, we first mean-normalized the data and identified highly variable genes from
956 the wild type AB and RNF datasets (minimum of 3 transcripts per cell, minimum of 3 cells
957 expressing gene, minimum V-score percentile of 85%). We then Z-scored counts for each gene
958 and performed principal component analysis (PCA) with 50 components. Cells from the spock1
959 mutant libraries were projected into the same principal component subspace. A k-nearest
960 neighbor graph (k=10) was generated based on the Euclidean distance in gene expression
961 between cells within this subspace. The Leiden algorithm was used to cluster cells into
962 subgroups(Traag et al., 2019). The neighborhood graph was embedded and visualized using

963 UMAP and the data was explored interactively with SPRING(Weinreb et al., 2017) to aid in cell
964 cluster annotation.
965
966 Cells belonging to the liver, pharyngeal arches, skin, and muscle were removed prior to differential
967 gene expression (DGE) analysis. The filtered dataset was reanalyzed using the methods
968 described above. The Wilcoxon rank-sum test was used to generate a list of potential genes that
969 are differentially regulated (fold change > 2) between genotypes across each Leiden cluster
970 (Table S2). Genes were only considered for DGE analysis if they were expressed in at least 5%
971 of cells in a given cluster and had a minimum mean of 10 transcripts per cell. Cells belonging to
972 the AB and RNF background were treated as a single wild type genotype for the analysis. The
973 vascular cluster (Leiden 13) was subclustered and similarly analyzed for DGE (Table S3).
974
975 **Data availability**
976 The raw reads from the counts matrix and associated metadata from the single-cell experiments
977 have been deposited to GEO.
978
979 All code for the single-cell analysis is available as interactive Jupyter notebooks here:
980 https://github.com/AllonKleinLab/paper-data/tree/master/OBrown2021_ZebrafishBBB
981
982 Interactive exploration of the full single-cell data can be found here:
983 https://kleintools.hms.harvard.edu/tools/springViewer_1_6_dev.html?client_datasets/2021_OBr
984 own/2021_OBrown
985
986 Exploration of the vascular subcluster cells can be found here:
987 https://kleintools.hms.harvard.edu/tools/springViewer_1_6_dev.html?client_datasets/2021_OBr
988 own_Vasculature/2021_OBrown_Vasculature

989 **Supplemental Figures**

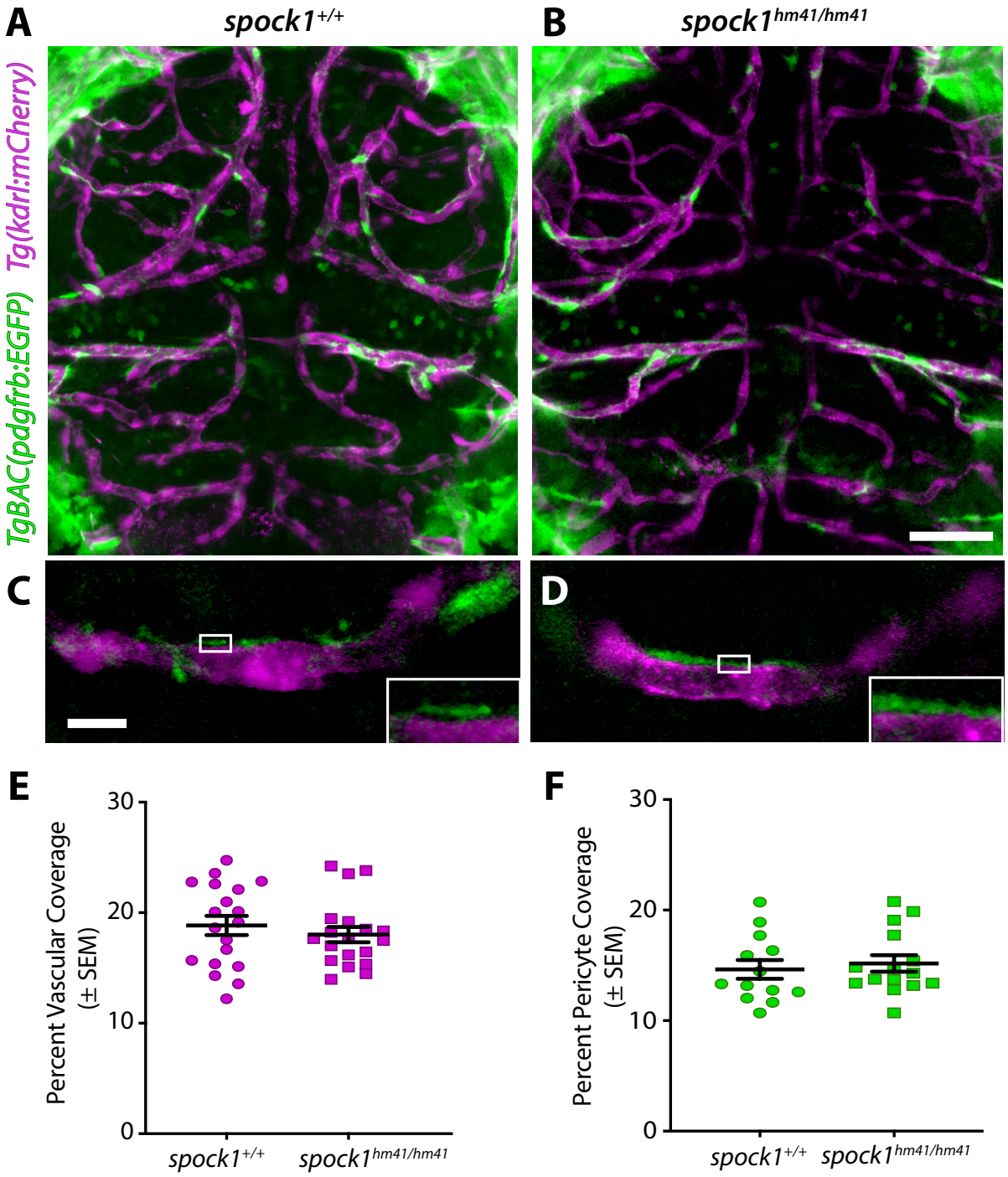

990

991 **Figure S1. *Spock1*$^{hm41/hm41}$ mutants have normal vascular patterning.** (**A-B**) Dorsal maximum
992 intensity projection of 5 dpf wild type (**A**) and mutant (**B**) brains with endothelial cells marked by
993 the kdrl:mCherry transgene (magenta) and pericytes marked by the pdgfrb:EGFP transgene
994 (green). (**C-D**) Zoomed in view of vessels reveals diminished basement membrane between

995 pericytes (green) and vessels (magenta) in mutants (**D**) compared to wild type siblings (**C**). This
996 is further highlighted in the higher magnification insets, with a visible gap present in the wild type
997 vessel (**C**) but not in the mutants (**D**). (**E-F**) Quantification of total vascular coverage of the brain
998 (kdrl:mCherry+ area/total brain area, **E**) and total pericyte coverage of the vasculature
999 (pdgfrb:EGFP+ area/kdrl:mCherry+ area, **F**), with each individual fish marked by a single point.
1000 Scale bars represent 50 μm (**B**) and 10 μm (**C**). T-test comparison reveals no significant difference
1001 between wild type and mutant fish for either vascular or pericyte coverage.

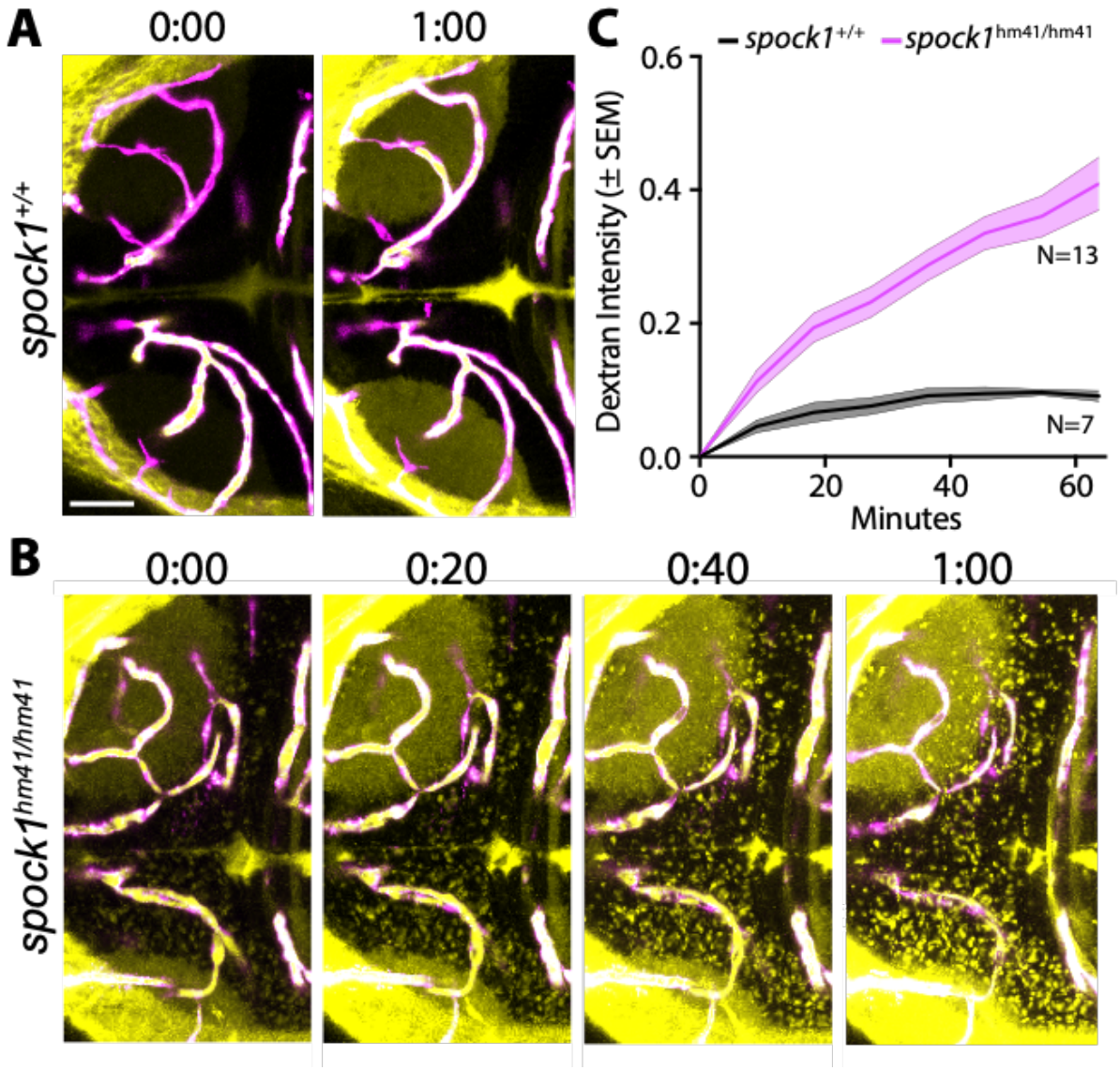

1002

1003 **Figure S2. Time lapse imaging reveals leakage dynamics in *spock1*$^{hm41/hm41}$ mutants.** (**A-**
1004 **B**) Dorsal maximum intensity projection of a wild type (A) and *spock1*$^{hm41/hm41}$ mutant (B) midbrain
1005 reveals steady accumulation of 10 kDa Dextran (yellow) outside of the vasculature (magenta)
1006 over the course of one hour in *spock1* mutants. (**C**) Quantification of Dextran accumulation in the
1007 midbrain parenchyma outside of the vasculature over time in wild type fish (black line) and
1008 *spock1*$^{hm41/hm41}$ mutants (magenta line). Scale bar represents 50 µm.

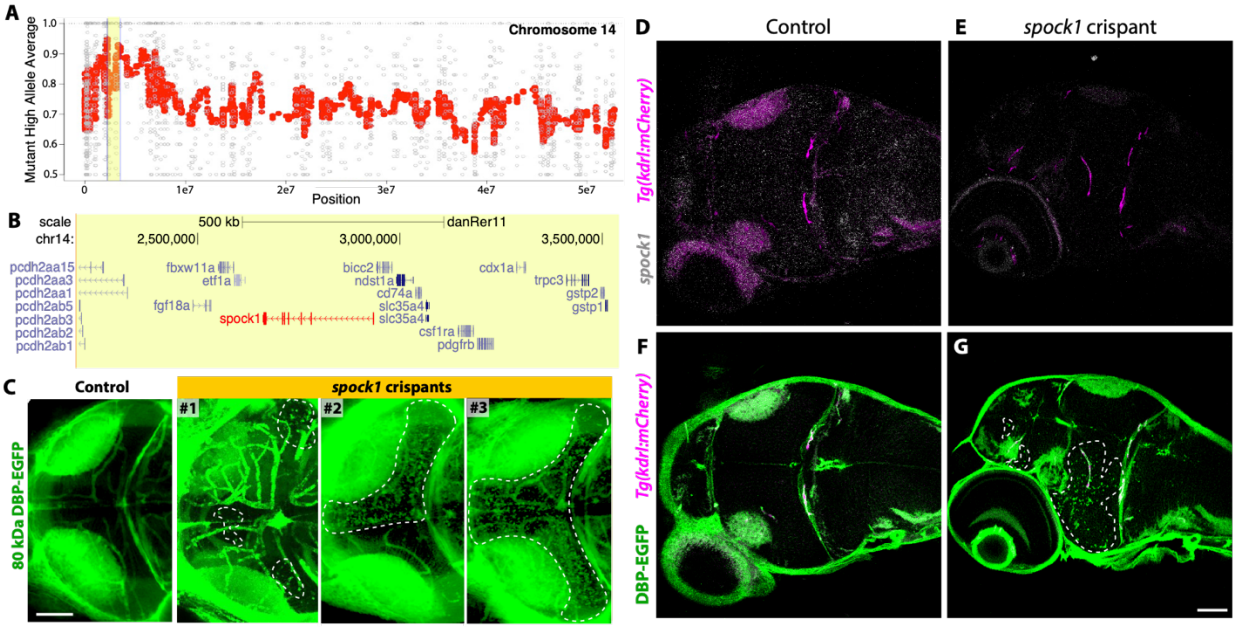

Figure S3. Leaky phenotype maps to *spock1* gene on chr14:2205271-3513919. (**A**) Manhattan plot of linkage on chromosome 14 with the average mutant alleles per 20 neighbors plotted in red. The region of highest linkage is highlighted in yellow. (**B**) Genome browser view of the highest linked region to the leaky phenotype. Eight of the genes within this region were expressed in the 5 dpf bulk RNAseq data: *fgf18a, spock1, bicc2, csf1ra, ndst1a, slc35a4, gstp1* and *gstp2*. Two of these genes were differentially expressed in leaky mutants compared to wild type (*csf1ra* and *gstp2*) and *spock1* (marked in red) had several SNPs that completely segregated in the leaky fish. (**C**) Mosaic *spock1* crispants display increased leakage of the transgenic DBP-EGFP tracer outside of the vasculature (outlined by white dashed line). (**D-E**) Dorsal view of whole mount HCR in situ for *spock1* (white) reveals expression throughout the brain of uninjected controls (D) but not in *spock1* crispants (E). (**F-G**) While controls confine the DBP-EGFP tracer (green) within the blood vessels (magenta) in the brain (F), *spock1* crispants display increased leakage into the brain parenchyma (G, outlined by white dashed line), corresponding with the loss of *spock1* expression (E). Scale bars represent 50 μm.

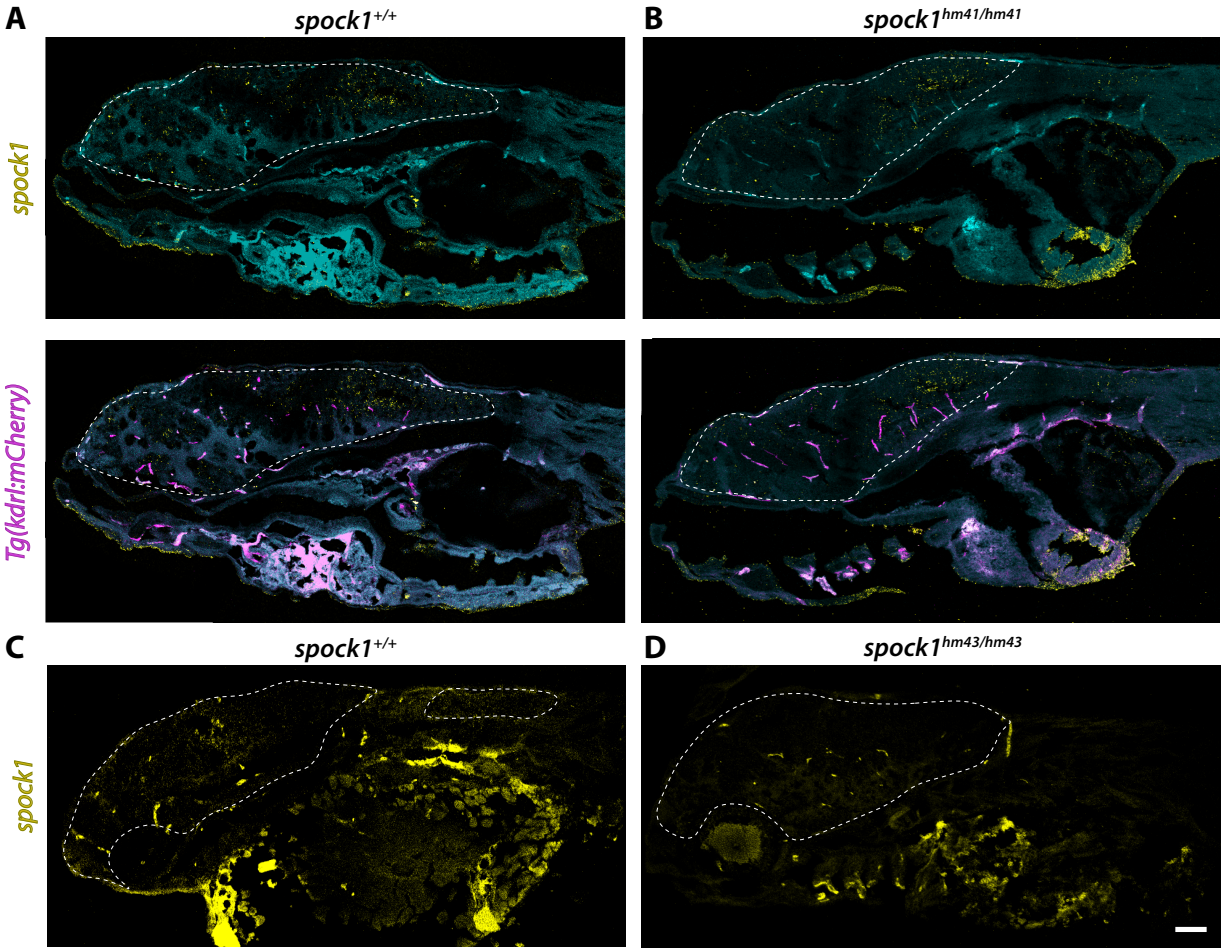

Figure S4. Expression of *spock1* is unaltered in *spock1*$^{hm41/hm41}$ mutants and absent in *spock1*$^{hm43/hm43}$ mutants. (**A-B**) *Spock1* expression (yellow) is found throughout the brain and spinal cord (outlined by a white dashed line) in wild type (A) and *spock1*$^{hm41/hm41}$ mutant fish (B) at 5 dpf. *Spock1* expression never colocalizes with vascular *Tg(kdrl:mCherry)* expression (magenta). Tissue autofluorescence is depicted in turquoise. (**C-D**) Unlike *spock1*$^{hm41/hm41}$ fish and wild type fish (C), *spock1*$^{hm43/hm43}$ mutants, which completely lack the 5' UTR and start codon of *spock1*, do not have any detectable *spock1* expression in the brain (D). The remaining signal in the yolk and blood vessels is due to tissue autofluorescence. Scale bar represents 50 μm.

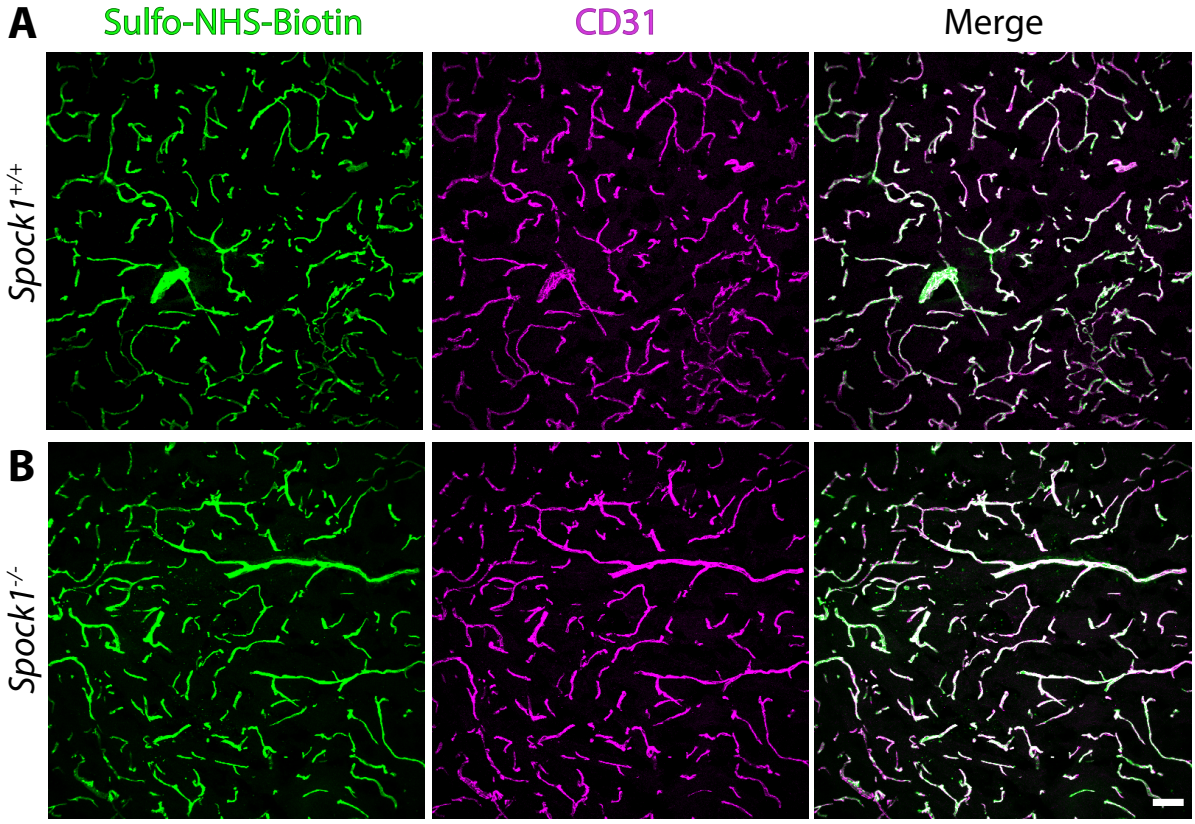

1034

1035 **Figure S5. Adult *Spock1*$^{-/-}$ mice recover BBB function.** (**A-B**) Tracer leakage assays in adult
1036 wild type (A) and *Spock1*$^{-/-}$ mice (B) reveals that both genotypes confine the injected Sulfo-NHS-
1037 Biotin tracer (green) within the CD31+ vasculature (magenta), indicating a functional BBB. Scale
1038 bar represents 50 μm.

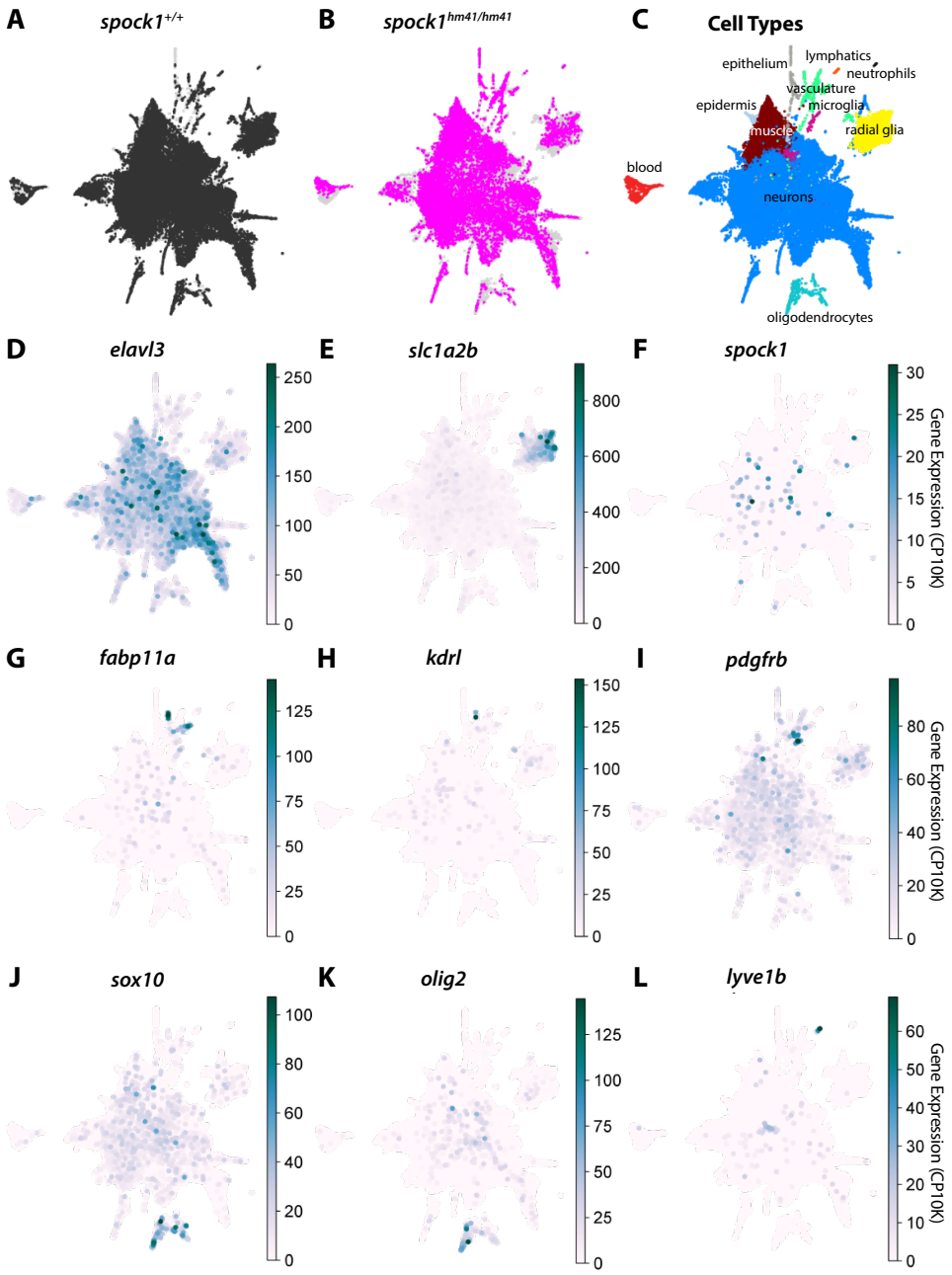

Figure S6. scRNA-seq captures all neurovascular cells in both mutant and wild type larvae. (**A-B**) UMAP of the whole brain dataset separated shows overlap between wild type (A) and *spock1*$^{hm41/hm41}$ mutant (B) cell type coverage, indicating that no cell type is absent in the mutant background. (**C**) UMAP of the total data set separated by annotated cell type, with the vast majority of sequenced cells being neuronal (blue). Our data does capture blood cells (red), microglia (magenta), oligodendrocytes (aqua), radial glia (yellow), and vascular cells (green). (**D-L**) Gene expression plots for *elavl3* (D) for neurons, *slc1a2b* (E) for radial glia, *fabp11a* (G) and *kdrl* (H) for endothelial cells, *pdgfrb* (I) for pericytes and neurons, *sox10* (J) and *olig2* (K) for

1048 oligodendrocytes, and *lyve1b* (L) for lymphatic endothelial cells reveals that *spock1* (F) is primarily
1049 expressed by neurons and absent from the vascular cells.